Marine and Petroleum Geology 112 (2020) 104038

Contents lists available at ScienceDirect

Marine and Petroleum Geology

journal homepage: www.elsevier.com/locate/marpetgeo

Research paper

Carboniferous graben structures, evaporite accumulations and tectonic inversion in the southeastern Norwegian Barents Sea

Muhammad Hassaan[a,b,*], Jan Inge Faleide[a,b], Roy Helge Gabrielsen[a], Filippos Tsikalas[c,a]

[a] Department of Geosciences, University of Oslo, P.O. Box 1047, Blindern, NO-0316, Oslo, Norway
[b] Research Centre for Arctic Petroleum Exploration (ARCEx), University of Tromsø, Hansine Hansens veg 18, NO-9019, Tromsø, Norway
[c] Vår Energi AS, P.O. Box 101 Forus, NO-4068, Stavanger, Norway

ARTICLE INFO

Keywords:
Southeastern Barents Sea
Tectono-stratigraphic evolution
Carboniferous basins
Evaporites
Domes
Salt wall
tectonic inversion

ABSTRACT

High quality reprocessed seismic reflection profiles and available wells were used to study the little studied southeastern Norwegian Barents Sea and east Finnmark Platform. The study area comprises prominent structural elements such as the Haapet, Veslekari, and Signalhorn domes, the West Fedynsky High, and the Tiddlybanken and Nordkapp basins. Seven deep-seated Carboniferous grabens, not formally described earlier, were defined and informally named; and similarly, five evaporite bodies that are tapered stratigraphically above the grabens have been mapped in detail. In the late Devonian, the region comprised a central structural high (Fedynsky High), and two depressions to the north and south, and has subsequently experienced transtensional deformation during a late Devonian-early Carboniferous NE-SW regional extensional phase. As a result, a NW-SE trending graben system was created over the paleotopography, following the inherited Timanian orogeny lineaments and giving rise to the deep-seated Carboniferous grabens. Pennsylvanian to early Permian evaporites were deposited and were characterized by mobile and non-mobile lithologies. The Carboniferous structures controlled the volume, thickness and lithological alterations of the evaporites, and have later influenced the distribution and development of the salt wall and domes. The Haapet, Veslekari, composite West Fedynsky (two domes informally named Alpha and Beta) and Signalhorn domes were generated and the salt wall of the Tiddlybanken Basin was rejuvenated during the late Triassic due to compressional stresses propagating from the evolving Novaya Zemlya fold-and-thrust belt. The domes and salt wall were subsequently reactivated during the upper Jurassic and earliest Cretaceous. Furthermore, we infer that the main phase of reactivation of these structures took place during the early-middle Eocene due to far-field stresses from the transpressional Eurekan/Spitsbergen orogeny.

1. Introduction

While the tectono-stratigraphic development of the southwestern Barents Sea is generally well established, the southeastern Norwegian Barents Sea (Fig. 1) was only considered for hydrocarbon exploration in the last few years (e.g. Mattingsdal et al., 2015). In this context, the geologic understanding of the southwestern Barents Sea is well constrained and the area was influenced by multiple orogenic events, followed by rifting and tectonic inversion (e.g. Faleide et al., 1984; Faleide et al., 2008; Faleide et al., 1993; Gabrielsen et al., 1990; Gudlaugsson et al., 1998). Furthermore, several studies have provided details on basin initiation, basin evolution and architecture as well as structural reactivation for the region (e.g. Gabrielsen, 1984; Gabrielsen et al., 1997; Ronnevik et al., 1982).

The southeastern Norwegian Barents Sea is relatively less well explored. It comprises several basins, platforms and structural highs, some of which include salt structures (Dellmour et al., 2016; Gernigon et al., 2018; Mattingsdal et al., 2015; Rojo et al., 2019; Rowan and Lindsø, 2017) (Fig. 1). The study area, which is situated within the southeastern Norwegian Barents Sea and nearby east Finnmark Platform, straddles the boundaries of the eastern and western parts of the Barents Shelf that are underlain by different basement units of contrasting structural grains (e.g. Drachev et al., 2010; Faleide et al., 2018; Gernigon et al., 2018; Gernigon et al., 2014) (Fig. 1). Located at such structural terrain transition, the study area has recorded a complex geological history (e.g. Gee et al., 2006; Henriksen et al., 2011a). Although several licenses have been recently awarded in the region, exploration in the southeastern Norwegian Barents Sea and east Finnmark Platform is still

* Corresponding author. Department of Geosciences, University of Oslo, P.O. Box 1047, Blindern, NO-0316, Oslo, Norway.
E-mail addresses: muhammad.hassaan@geo.uio.no (M. Hassaan), j.i.faleide@geo.uio.no (J.I. Faleide), r.h.gabrielsen@geo.uio.no (R.H. Gabrielsen), filippos.tsikalas@geo.uio.no (F. Tsikalas).

https://doi.org/10.1016/j.marpetgeo.2019.104038
Received 30 May 2019; Received in revised form 5 September 2019; Accepted 6 September 2019
Available online 09 September 2019

in its infancy. The region lacks adequate deep-target commercial wells, and thus depends largely on quality seismic reflection profiles to determine the timing of tectonic events, sediment distribution and thickness.

In the present study, we use recently acquired and re-processed seismic reflection datasets tied to available wells in the east Finnmark Platform. Through seismic and structural interpretations, we define the inherited structural grain, the configuration of newly identified grabens

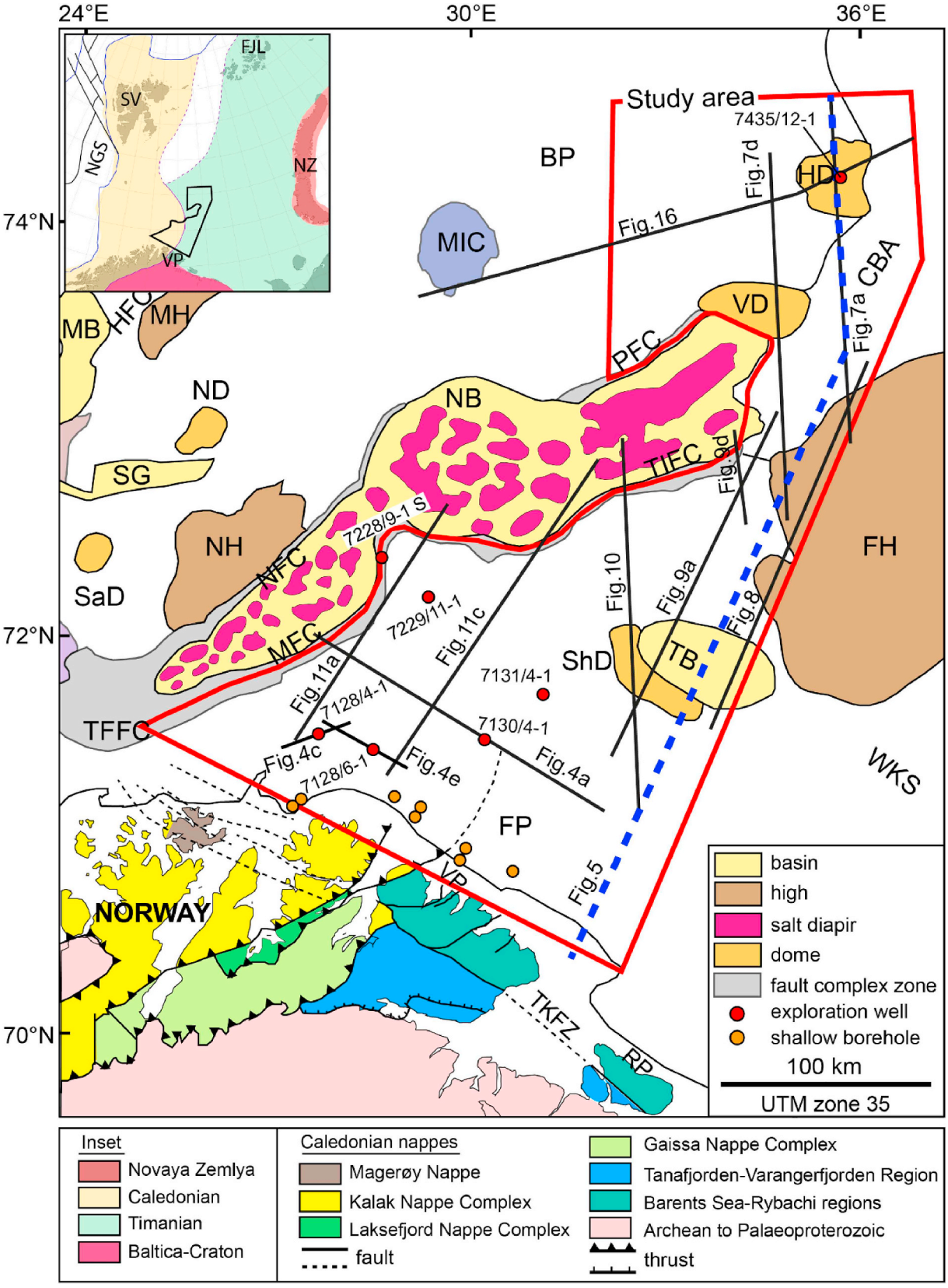

(caption on next page)

Fig. 1. Main structural elements of the central and southeastern Norwegian Barents Sea (modified from: offshore, Mattingsdal et al., 2015; onshore, Sigmond, 2003), and study area denoted by the red polygon. Selected seismic profiles and the regional composite profile in various figures are shown in black and dotted blue lines, respectively. Inset: location of the study area at the transition between the Timanian and Caledonian structural fabrics. BP: Bjarmeland Platform; CBA: Central Barents Arch; FH: Fedynsky High; FJL: Franz Joseph Land; FP: Finnmark Platform; HD: Haapet Dome; HFC: Hoop Fault Complex; MB: Maud Basin; MFC: Måsøy Fault Complex; MH: Mercurius High; MIC: Mjølnir Impact Crater; NB: Nordkapp Basin; ND: Norvarg Dome; NGS: Norwegian-Greenland Sea; NH: Norsel High; NZ: Novaya Zemlya; PFC: Polstjerna Fault Complex; RP: Rybachy Peninsula; SaD: Samson Dome; ShD: Signalhorn Dome; SG: Swaen graben; SV: Svalbard; TD: Tiddlybanken Basin; TFFC: Troms-Finnmark Fault Complex; TIFC: Thor Iversen Fault Complex; TKFZ: Trollfjorden-Komagelva Fault Zone; VD: Veslekari Dome; VP: Varanger Peninsula; WKS: West Kola Saddle. (For interpretation of the references to colour in this figure legend, the reader is referred to the Web version of this article.)

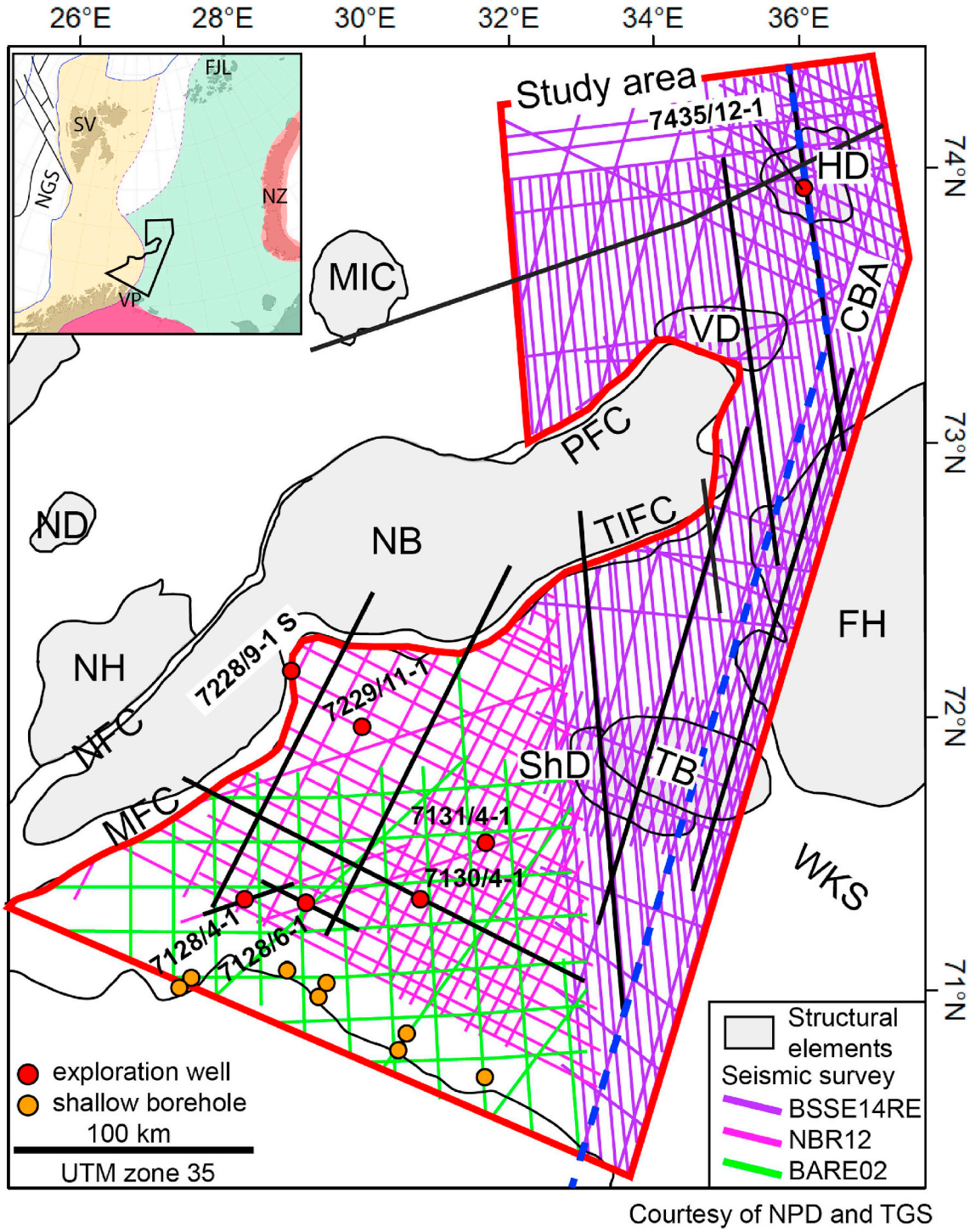

Fig. 2. Utilized seismic reflection dataset, exploration wells and shallow boreholes (Bugge et al., 1995) within the study area (thick red polygon), overlaid on the main structural elements. Inset, selected seismic profiles shown in various figures, and abbreviations as in Fig. 1. (For interpretation of the references to colour in this figure legend, the reader is referred to the Web version of this article.)

and the orientation of the paleo-stress regime. We refine the character (mobile and non-mobile) and expression of relevant evaporite bodies. Furthermore, we describe the inverted structures, investigate the relation between the deep-seated graben structures and structural reactivation of the domes and salt wall. The current study also documents the observations related to the influence of the tectonic inversion and far-field regional stresses.

2. Data

The seismic database comprises conventional 2D multi-channel seismic (MCS) reflection profiles covering an area of ~72,000 km^2 (Fig. 2; Table 1a–b). The database consists of three seismic surveys, namely BSSE14RE, NBR12 and BARE02 that have an average line spacing of 4 km, 6 km and 15 km, respectively. The BSSE14RE survey covers the entire southeastern Norwegian Barents Sea including the northern Nordkapp Basin. The interpreted parts of the two other surveys, NBR12 and BARE02, cover the east Finnmark Platform (Fig. 2).

Three deeply penetrating exploration wells 7130/4-1, 7128/4-1 and 7128/6-1 (Figs. 1 and 2) are located on the east Finnmark Platform and have been utilized in the present study together with available information from shallow stratigraphic boreholes in the southern part of east Finnmark Platform close to Norwegian mainland (Bugge et al., 1995). The available wells have been used to define well-to-seismic ties and time-to-depth conversion, and to guide the seismic interpretation. Although the confidence of age constraints is naturally somewhat reduced due to limited number of wells, long distance between wells and seismic profile line-spacing (Table 1a), we are confident of the provided interpretations due to the good quality of the available seismic reflection profiles.

3. Geological setting

The Paleozoic evolution of the greater Barents Sea was influenced by the Timanian Orogenesis of late Neoproterozoic age (Barrère et al., 2009, 2011) (Fig. 1, inset). The Timanian Orogeny formed a fold-and-thrust belt along the northeastern passive margin of Baltica and its offshore domain (e.g. Gee et al., 2008; Kostyuchenko et al., 2006; Roberts and Olovyanishnikov, 2004; Roberts and Siedlecka, 2002). Imprints of the NW-SE to N-S striking Timanide Orogen can be traced from the southern polar Urals to the Varanger Peninsula in northern Norway, extending into the eastern Barents Sea. In contrast, the Caledonian structural grain is dominantly NE-SW in the southernmost Barents Sea (e.g. Gernigon and Brönner, 2012; Ritzmann and Faleide, 2007) and turns into NNW-SSE northwards (Gernigon and Brönner, 2012). The age relations and the exact geographical position of the transition from Timanian to Caledonian structural grains are not well constrained in all parts of the Barents Sea region (e.g. Breivik et al., 2005; Breivik et al., 2002; Faleide et al., 2018; Gee et al., 2006; Ritzmann and Faleide, 2007), but the transition is probably situated between Svalbard and Franz Josef Land (Barrère et al., 2009; Henriksen et al., 2011a; Klitzke et al., 2019; Marello et al., 2013; Pease et al., 2001, 2014; Shulgin et al., 2018). However, Timanian basement is believed to underlie the central/eastern Barents Sea as supported by drill-core data from Franz Josef Land (Pease et al., 2001) and regional offshore geophysical data (Gernigon et al., 2014; Marello et al., 2010, 2013; Ritzmann and Faleide, 2007, 2009). In parallel, it has been suggested that the interference between Timanian and Caledonian fold structures has caused an apparent double-fold pattern on the Norwegian mainland (Herrevold et al., 2009).

The Caledonian basement fabric (Silurian-Devonian) shaped the western Barents Sea and is overprinted by Paleozoic-Mesozoic basins and structural highs (Anell et al., 2016; Blaich et al., 2017; Faleide et al., 2018; Gabrielsen et al., 1990; Tsikalas et al., 2019). The Carboniferous basin system, as evidenced in regional seismic and gravity data (Breivik et al., 1995; Gabrielsen et al., 1990; Gudlaugsson et al., 1998), was likely influenced by the Timanides to the east (Faleide et al., 2018) and Caledonides to the west (Gernigon et al., 2014; Lippard and Roberts, 1987). During the late Carboniferous (Bashkirian), deposition took place in a warm, semi-arid to arid climate (Larssen et al., 2005). Thus, these stratigraphic successions were dominated by carbonates and evaporites that filled the regional horst-and-graben reliefs of the central and western Barents Sea (Gudlaugsson et al., 1998; Larssen et al., 2002, 2005). The NE-SW to NNE-SSW striking Nordkapp and Ottar basins (that include the Samson and Norvarg evaporite domes, were prominent structures during the accumulation of thick evaporite sequences (Breivik et al., 1995; Gabrielsen et al., 1992; Alves, 2016; Mattos et al., 2016; Rowan and Lindsø, 2017) (Fig. 1). Subsequently, late Permian-early Triassic subsidence provided accommodation space for large volumes of sediment that prograded into the southeastern Barents Sea - sourced from the Uralides and the south Baltic Shield (Glørstad-Clark et al., 2010; Riis et al., 2008). By late Triassic, the prograding system reached Svalbard causing deposition of several transgressive-regressive cycles of marine, deltaic and continental clastic sediment (Glørstad-Clark et al., 2010; Klausen et al., 2015).

Regional extension took place in the southwestern Barents Sea from the late Jurassic to early Cretaceous and led to further subsidence, accentuating the subsidence levels of the deep basins in the west from the shallow basins in the east (Faleide et al., 1993, 2008; Gabrielsen et al., 1997; Henriksen et al., 2011a; Indrevær et al., 2017). During the late Cretaceous to the Paleocene, narrow pull-apart basins developed along a mega-shear system (De Geer Zone) at the western Barents Sea-

Table 1
(a) Utilized seismic reflection dataset, (b) calculated vertical seismic resolution.

(a)

Survey	Year	Company/ Authority	Record time (twt, s)	Profile (km) [within study area]
BSSE14-RE	2014	NPD/TGS	9	~18,600
NBR-12	2012	NPD	10	~8000
BARE-02	2002	NPD	6	~3000

(b)

Zone		Frequency (Hz) (F)	Velocity (m/s) (V)	Wavelength (m) (λ = V/F)	Vertical resolution (m) (λ/4)
Shallow	Cretaceous	50	2335	47	12
Deep	Permian to Pennsylvanian	15	6280	419	105
		20	6280	314	79
	Mississippian	15	4960	331	83
		20	4960	248	62

Svalbard margin (Faleide et al., 1993; Knutsen and Larsen, 1997; Kristensen et al., 2018; Lasabuda et al., 2018a; Ryseth et al., 2003). Eventually, tectonic stress was transferred from the east towards the west, leading to the opening of the Norwegian-Greenland Sea during the Paleocene-Eocene transition (Eldholm et al., 2002; Faleide et al., 2008; Tsikalas et al., 2012). Subsequently, the western Barents Sea margin was affected and shaped by the multiphase Eurekan orogenic deformation during the early Cenozoic (Leever et al., 2011; Piepjohn et al., 2016). During the Neogene, the entire Barents Shelf experienced uplift and erosion related to Plio-Pleistocene glaciations (Baig et al., 2016; Green and Duddy, 2010; Henriksen et al., 2011b). However, pre-glacial uplift is also considered to have affected the western and northern parts of the Barents Sea (Dimakis et al., 1998; Lasabuda et al., 2018b; Zattin et al., 2016).

4. Tectono-stratigraphic evolution: new insights

4.1. Tectono-stratigraphic scheme and interpretations

Seismo-stratigraphic markers were tied to wells 7130/4-1, 7128/4-1 and 7128/6-1 on the east Finnmark Platform and were also correlated to the shallow boreholes in the area (Figs. 1 and 2) (Bugge et al., 1995). Formation tops from these wells were used for the sub-division of the Paleozoic strata on the Finnmark Platform (Fig. 3). As no deep penetrating well has yet been drilled within the southeastern Norwegian Barents Sea, we have utilized the seismic reflection datasets to correlate the Upper Paleozoic stratigraphy and structures. Five seismic sequences bounded by six key horizons were mapped and the utilized litho- and chrono-stratigraphic scheme is shown in Fig. 3. Time-structure surfaces were generated in order to get a better understanding of the lateral and vertical configuration of stratigraphic units, as well as to visualise the tectono-stratigraphic evolution. In this context, seismic sections are used to illustrate detailed observations.

The base Carboniferous? (BCa?) and top Serpukhovian (TS) reflections are non-continuous, and disturbances due to the loss of high frequencies with depth, the burial depth of the studied interval, the type of the imaged strata and also multiples increase significantly with depth. Together with the top of the Permian (TP), the above reflections are found to bound two sequences, the late Devonian to Mississippian and the Pennsylvanian to Permian sequences, respectively (Fig. 3). Data resolution depreciates below the evaporite sequence of the Gipsdalen Group of Pennsylvanian to early Permian age (Fig. 3). The seismic reflections of the top Permian (TP), the middle Jurassic (MJ) and the Base Cretaceous Unconformity (BCU) were interpreted with high confidence because these reflections are continuous with prominent seismic acoustic impedance contrasts. They bound three seismic sequences, namely Triassic-middle Jurassic, upper Jurassic and Cretaceous (Fig. 3).

We have further subdivided the Carboniferous seismic sequence into several units by the use of well 7130/4-1, 7128/4-1 and 7128/6-1 positioned at the NW margin of the Finnmark Platform (Fig. 4). Due to the fact that data quality locally deteriorates beneath evaporite-cored structures (pillows and salt walls), and no deep exploration well has been drilled in the upper Paleozoic sequence over or across salt structures, it was not possible to correlate the individual Carboniferous formations in the entire study area. Therefore, these are rather utilized for detailed observations and related discussion within the east Finnmark Platform.

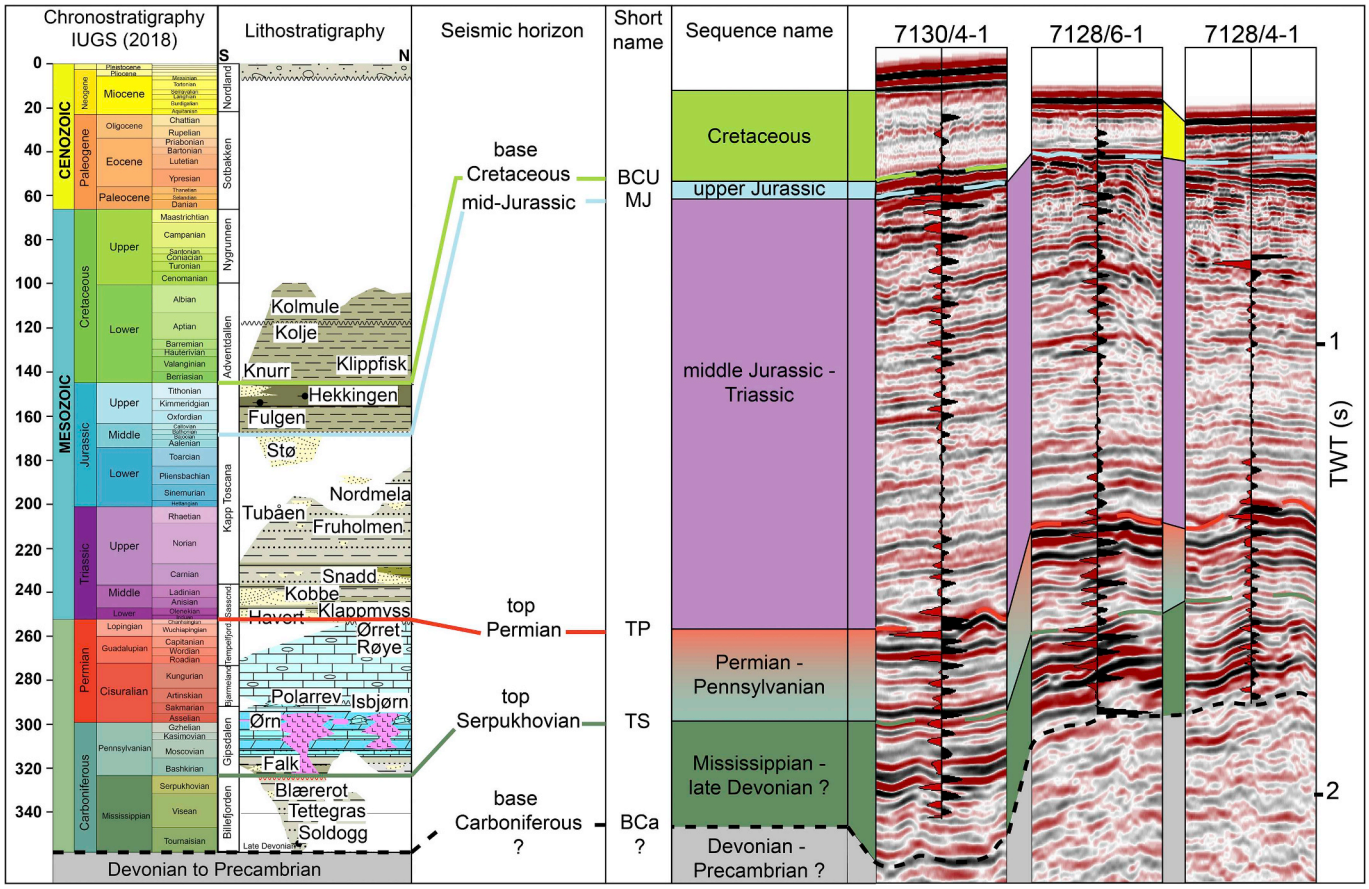

Fig. 3. Stratigraphic framework and key seismic horizons interpreted throughout the study area. Lithostratigraphy of the southeastern Norwegian Barents Sea based on Larssen et al. (2005) and modified after Gernigon et al. (2018). Locations of extracted seismic reflection panels with synthetic seismograms related to each well are indicated by red dotted boxes in Fig. 4a,c,e. (For interpretation of the references to colour in this figure legend, the reader is referred to the Web version of this article.)

4.2. Deep-seated Carboniferous grabens

The constructed composite type-profile, passing through all major regional structural elements, illustrates the structural and depositional basin configuration in the southeastern Norwegian Barents Sea (Fig. 5). The profile displays several deep-seated grabens affecting the Carboniferous level and demonstrates syn-tectonic (growth fault-related) deposition along NW-SE-striking master faults, following the Timanian trend. Several Carboniferous grabens are recognized and therefore informally named in this study (Fig. 6a). These are oriented NW-SE and orthogonally to the NE-SW trend of the Nordkapp Basin and other younger structural features, exhibiting contrasting structural spatial and temporal configurations, lateral extent and depth (relative to base level). Observed seismic facies in the southeastern Norwegian Barents Sea are also interpreted and described (Table 2). Descriptions of each of the newly discovered grabens are provided below (Table 3).

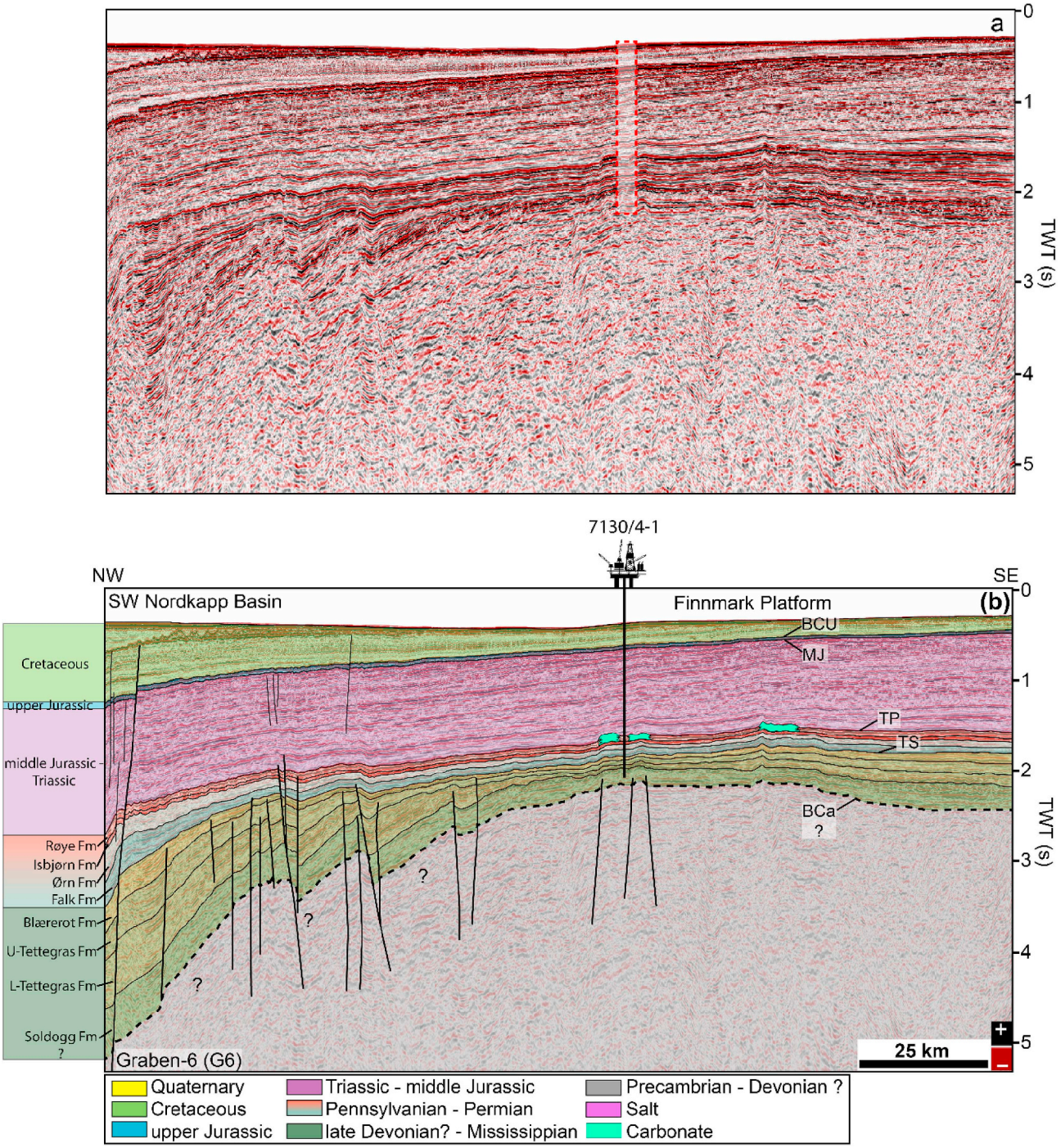

Fig. 4. Un-interpreted and interpreted seismic profiles illustrating well-to-seismic ties with (a–b) well 7130/4-1, (c–d) well 7128/4-1, and (e–f) well 7128/6-1. Locations of extracted seismic reflection panels with synthetic seismograms related to each well are indicated by red dotted boxes by red dotted boxes (see Fig. 3). Interpreted sequences include: Mississippian: Soldogg, Tettegras and Blærerot formations; Pennsylvanian to Permian: Falk, Ørn, Isbjørn, Røye formations; Triassic-middle Jurassic; upper Jurassic; and Cretaceous. Profile and well locations in Fig. 1. (g) Cores of upper Soldogg Formation from well 7128/4-1 illustrating continental siliciclastics, i.e. fluvial channel sandstones with minor amounts of finer grained siliciclastics and subordinate thin coal beds. (For interpretation of the references to colour in this figure legend, the reader is referred to the Web version of this article.)

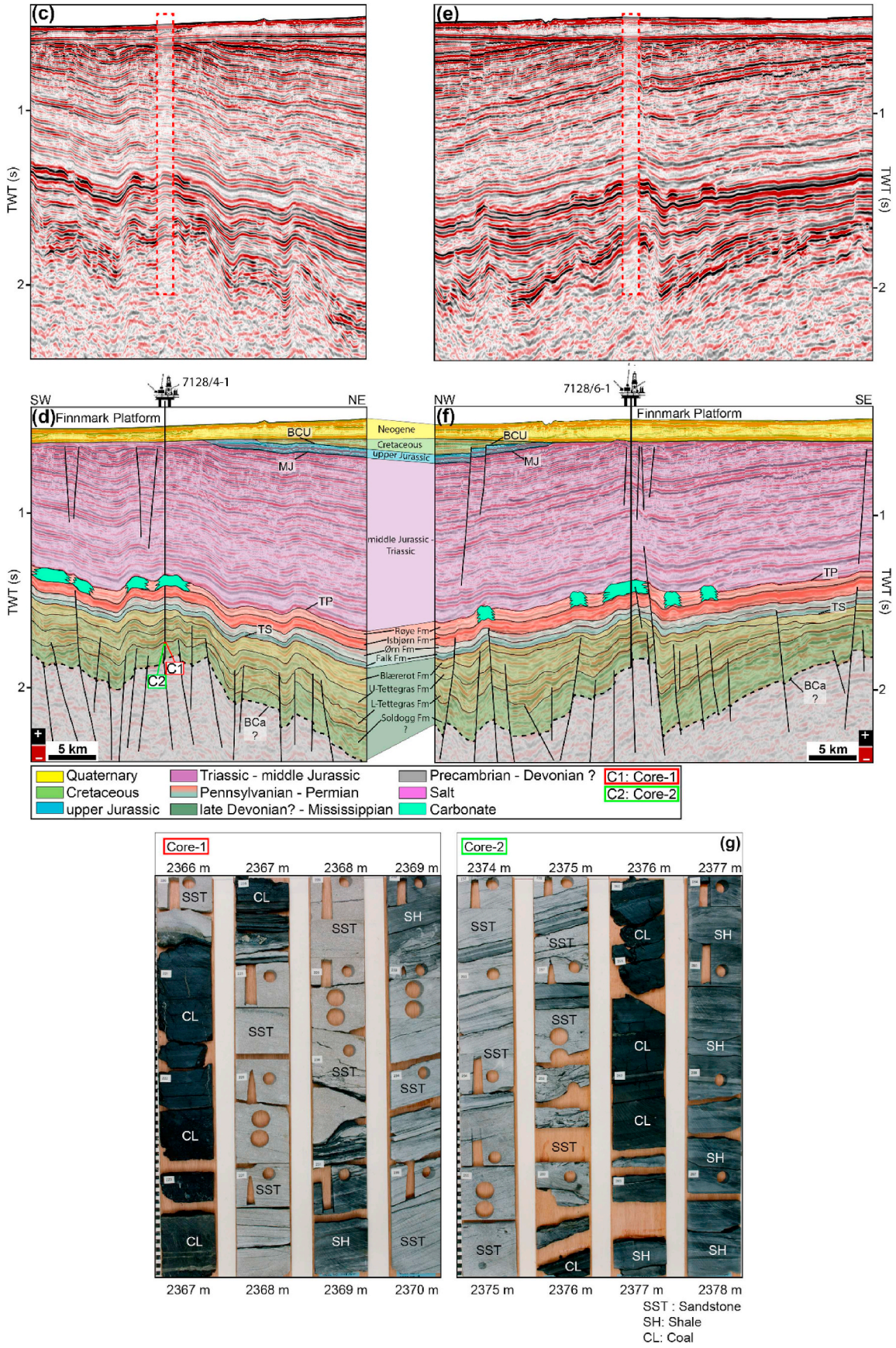

Fig. 4. (*continued*)

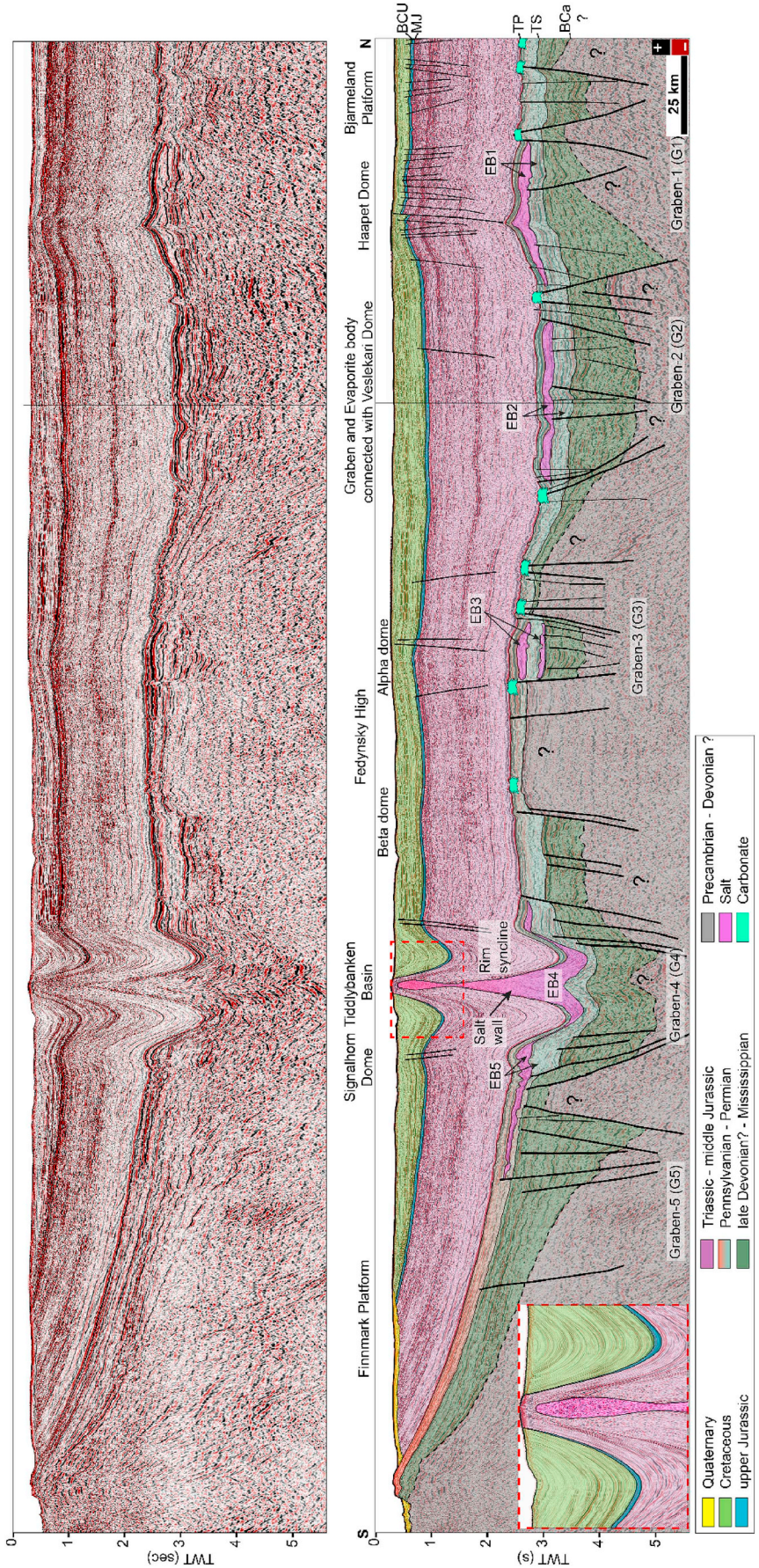

Fig. 5. Un-interpreted and interpreted composite seismic profile illustrating the main structural elements with focus on the deep-seated Carboniferous grabens G1-G5 and evaporite bodies EB1-EB5. Inset: part of the interpreted seismic profile on the rejuvenated salt wall of the Tiddlybanken Basin; rasters correspond to interpreted sequences (Fig. 3). Profile location in Fig. 1.

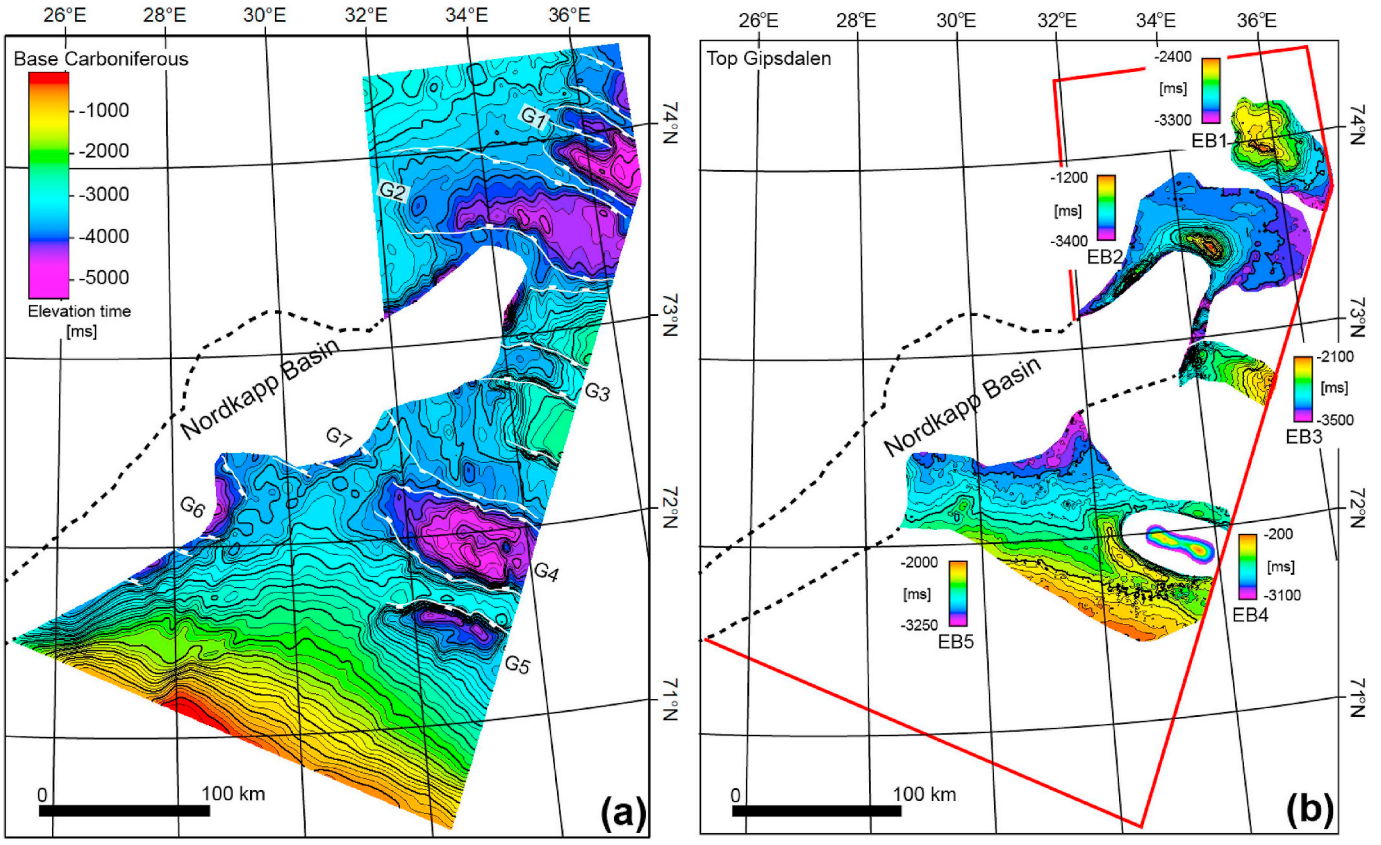

Fig. 6. (a) Base Carboniferous isochore time-structure map with emphasis on the NW-SE trending deep-seated grabens G1-G7, and **(b)** extent of the accumulated evaporite bodies EB1-EB5 at Top Gipsdalen level. Abbreviations as in Tables 2 and 3.

Table 2
Interpreted seismic facies.

Facies	Seismic characterization	Interpretation/location	Example
Carbonates			
SF4	Featureless and chaotic seismic reflections	Carbonates of the Bjarmeland Group, mound shaped morphological features and observed on the platform region and at the margins of the Carboniferous graben structures.	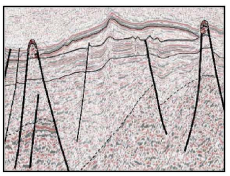
Evaporites			
SF3	Featureless and chaotic seismic reflections	Layered evaporites of the Gipsdalen Group, upper part of accumulated evaporites with mobile halite lithology and prominent features i.e. pillow and salt wall. Observed on Haapet, Veslekari, Signalhorn Dome, Fedynsky High, Tiddlybanken Basin and at the margins of the Nordkapp Basin.	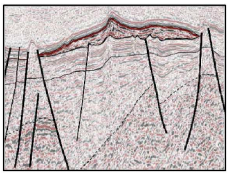
SF2	Semi-continuous, parallel to sub-parallel and medium to strong amplitude seismic reflections	Layered evaporites of the Gipsdalen Group, lower part of accumulated evaporites with inter-bedded, mixed non-halite and non-mobile lithologies i.e. anhydrite, gypsum. Observed on Haapet, Veslekari, Signalhorn Dome, Fedynsky High, Tiddlybanken Basin and at the margins of the Nordkapp Basin.	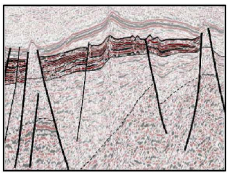
Clastic infill			
SF1	Semi-continuous, sub-parallel to diverging and medium amplitude seismic reflections	Clastic infill of the Billefjorden Group, observed on the Haapet Dome, Veslekari Dome, Fedynsky High, Signalhorn Dome, Tiddlybanken Basin, southeastern and central Nordkapp sub-basins.	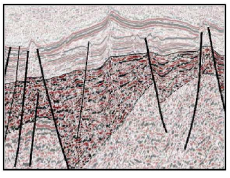

Table 3
Structural and morphological characteristics of the new defined deep-seated Carboniferous grabens.

Informal Name	Location	Master faults trend	Lateral extent (km)		Depth (ms)
			Length	Width	
Graben 1 (G1)	Haapet Dome	NW-SE	~74	~46	~4700
Graben 2 (G2)	Veslekari Dome	NW-SE	~130	~45	~4500
Graben 3 (G3)	Fedynsky High	NW-SE	~52	~23	~3600
Graben 4 (G4)	Tiddlybanken Basin/Signalhorn Dome	NW-SE	~98	~50	~4750
Graben 5 (G5)	Finnmark Platform	NW-SE	~75	~58	~4350
Graben 6 (G6)	southwestern Nordkapp Basin	NW-SE	unknown	~80	~5000
Graben 7 (G7)	central Nordkapp Basin	NW-SE	unknown	~60	~4750

4.2.1. Graben G1

NW-SE trending normal master faults dipping towards the axis of the structure constrain the graben G1 on both its flanks (Figs. 5, 6a and 7b; Table 3). Its southwestern graben margin is defined by a NW-SE trending horst, separating it from graben G2. Graben G1 changes in style along its strike, displaying a half-graben geometry in the northwestern part and a full-graben geometry in the southeastern part (Fig. 7b). The northern master fault has a pronounced antithetic fault on its basinward side that created a small graben structure (Fig. 7b). In the northwestern (half-graben) part the intra-graben seismic facies units have a wedge-shaped geometry and are composed of inclined, semi-continuous to sub-parallel and medium amplitude seismic reflections (SF1, Table 2). In the full-graben segment in the southeast, the seismic facies units exhibit flat, semi-continuous to sub-parallel and low amplitude seismic reflections (SF1, Table 2). The strata are dated as Mississippian age based on well data, and reaches a thickness of ~1500 ms two-way travel-time (twt) (~4200 m) within the hanging-wall against the southern master fault, which dips to the north (in the northwestern half-graben segment) (Fig. 7b). These are interpreted to be continental siliciclastic strata of the Billefjorden Group based on well correlation and seismic interpretation (Figs. 3 and 4g) that were deposited under humid, warm and terrestrial depositional conditions

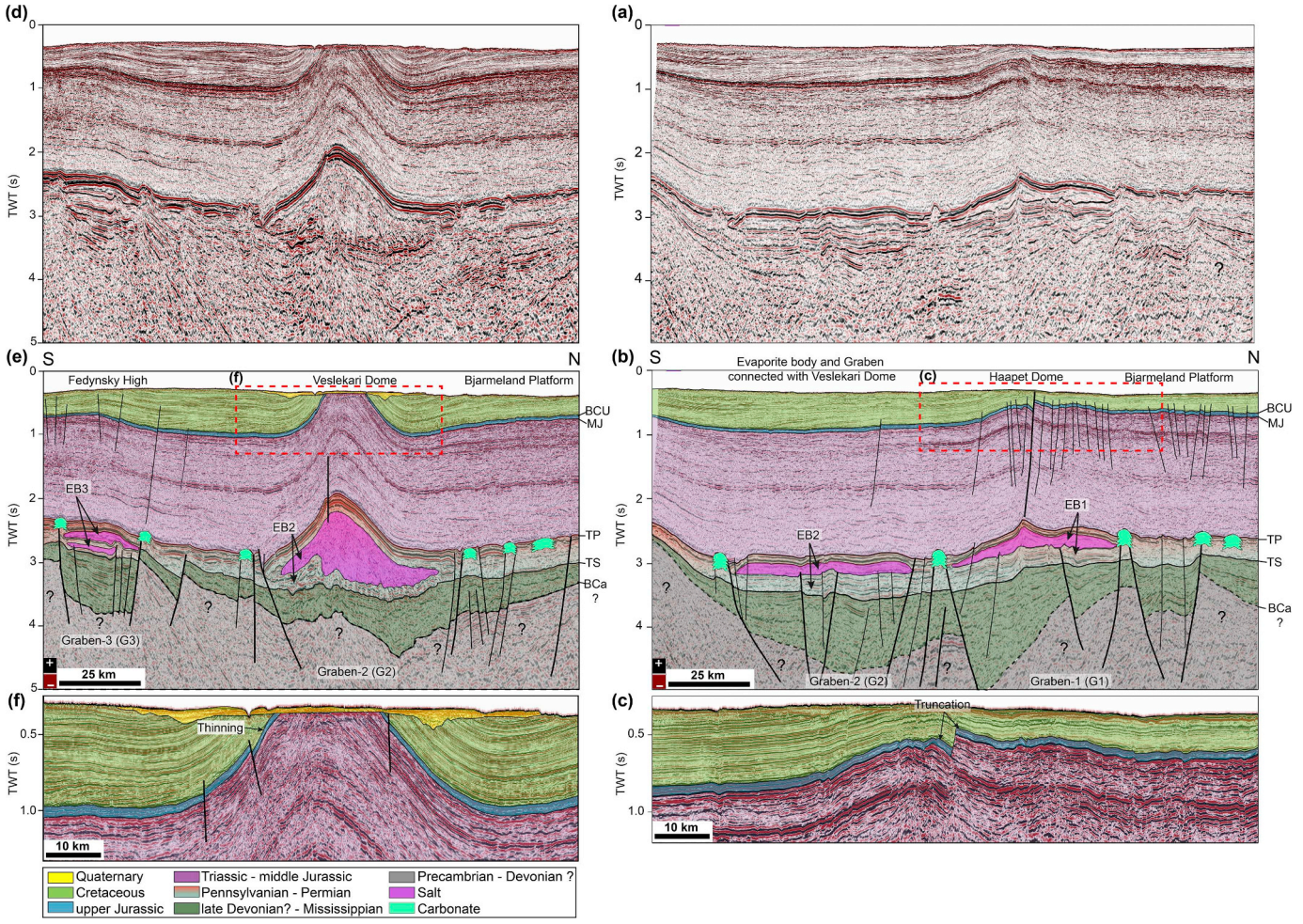

Fig. 7. (a–b) Un-interpreted and interpreted seismic profile, respectively, elucidating the Bjarmeland Platform and Haapet Dome with emphasis on the Carboniferous grabens G1-G2 and evaporite bodies EB1-EB2, note and compare the graben G2 geometry and thin evaporite body EB2 with Fig. 7e; **(c)** extract of the seismic profile displaying truncation of upper Jurassic strata below BCU. **(d–e)** Un-interpreted and interpreted seismic profile, illustrating the Bjarmeland Platform, Veslekari Dome and Fedynsky High with focus on the Carboniferous grabens G2-G3 and evaporite bodies EB2-EB3; **(f)** extract of the seismic profile displaying thinning of upper Jurassic towards the Veslekari Dome; rasters correspond to interpreted sequences (Fig. 3). Profile location in Fig. 1.

during active faulting (Figs. 5, 6a and 7b).

4.2.2. Graben G2

Normal NW-SE-trending master faults bound the margins of graben G2, both facing to the axis of the structure (Figs. 5, 6a, and 7b-e; Table 3). Graben G2 displays variable along-strike geometry, and its central segment is characterized by a half-graben configuration with maximum throw to the north and a horst that separates it from the northeastern Nordkapp sub-basin (Figs. 6a and 7e). The northwestern and southeastern segments of graben G2 exhibit full-graben geometry, whereas the southeastern part of the graben connects to a tilted platform associated with the Fedynsky High (Figs. 5, 6a and 7b). The seismic facies units in the central part of the graben show wedge-shaped geometry and consist of inclined, semi-continuous to discontinuous and low amplitude seismic reflections (SF1) (Fig. 7e; Table 2). Seismic reflections become chaotic in some places, likely due to the salt structure above. However, in the northwestern and southeastern parts of the graben, seismic facies units are composed of semi-continuous to diverging and medium to low amplitude seismic reflections (SF1) (Fig. 7b; Table 2). During active faulting, thick (~1400 ms twt; ~3900 m) continental siliciclastic strata of the Billefjorden Group (based on well correlation and seismic interpretation) (Figs. 3 and 4g) were deposited in the southeastern full-graben part (Fig. 7b).

4.2.3. Graben G3

The prominent Fedynsky High is a positive structural feature that extends across the border to Russia and possesses the shallowest depth with less faulted and eroded surface morphology at the base Carboniferous level (Figs. 5, 6a and 8b and 9b; Table 3). On the eastern limit of the study area, the high is mostly unaffected by faulting and contains only a narrow graben, informally named graben G3, that has a symmetric full-graben geometry (Fig. 8b). NW-SE-striking master faults border the graben and dip towards the axis of the structure. Overall, graben G3 deepens from southeast to northwest and geographically connects to the northeastern Nordkapp Basin (Fig. 6a). Internally, the seismic facies units constitute semi-continuous to discontinuous and medium to low amplitude seismic reflections (SF1, Table 2). During the Mississippian fault activity, continental siliciclastic strata of the Billefjorden Group (based on well correlation and seismic interpretation) with thickness of ~600 ms twt (~1600 m) were deposited (Fig. 3). The southern part of the Fedynsky High within the study area is less affected by NW-SE trending faults in comparison to the part farther north of graben G3 that exhibits thin Mississippian strata deposition with faulting (Figs. 5 and 8b). Occasionally, Mississippian successions show considerable growth in the hanging-wall against the normal faults to the north of graben G3 caused by active faulting (Fig. 7e). Towards the west, graben G3 shows similar internal geometry, while the Fedynsky High demonstrates more faulting (NW-SE trending) and tilted fault-block configuration with average normal throws of ~100–250 ms twt (~280–700 m) (Fig. 9b and e). At the boundary between the Fedynsky High and the northern Nordkapp Basin graben G3 appears to be more deformed (Fig. 9e).

4.2.4. Graben G4

Graben 4 is located south of the Fedynsky High and a relatively flat platform south of the high (Figs. 5, 6a and 8b; Table 3). It contains few NW-SE striking normal faults with moderate throws and accommodates ~600 ms twt (~1600 m) thick Mississippian strata. The seismic facies related to this stratigraphic unit shows discontinuous to semi-continuous and sub-parallel seismic reflections with medium amplitude strength (SF1) (Figs. 5 and 8b; Table 2). NW-SE striking master normal faults border graben G4 and dip towards the axis of the structure, creating full-graben geometry (Fig. 5). Graben G4 consists of numerous normal faults with horst-and-graben geometry and rotated fault-blocks (Figs. 9b and 10b). Internally, the seismic facies units consist of chaotic seismic reflections with high amplitude strength in the central part of the graben due to the salt wall (Figs. 5 and 9b). However, sediment architecture is better imaged towards the northwestern part of the graben (Fig. 10b). Here, the observed seismic facies units are composed of continuous to semi-continuous, sub-parallel and medium to low amplitude seismic reflections (SF1; Table 2). Mississippian strata with thickness of ~1400–1750 ms twt (~3900–4900 m) were deposited in the graben structure during active faulting.

4.2.5. Graben G5

Graben G5 is separated from graben G4 by a horst, which trends NW-SE. It is composed of a NW-SE striking normal boundary fault that dips towards the south. The master fault together with the shallowing of the hanging-wall towards the hinged margin in the south creates a half-graben wedge configuration (Figs. 5, 6a and 9b and 10b; Table 3). The sedimentary fill exhibits a wedge-shaped architecture with inclined, continuous to semi-continuous and medium amplitude seismic facies units (SF1, Table 2). Approximately ~1750 ms twt (~4900 m) thick continental siliciclastic strata of the Mississippian age Billefjorden Group (based on well correlation and seismic interpretation) (Figs. 3 and 4g) were deposited in the graben structure during active faulting (Fig. 10b). Mississippian successions tilt towards the southern hinged margin of the graben and subcrop close to the seafloor (Fig. 5).

4.2.6. Graben G6

Graben G6, together with graben G7, are located at the eastern margin of the NE-SW trending Nordkapp Basin where the evaporite layer is thin and thus seismic imaging is adequate to reveal pre-Pennsylvanian geometries. Graben G6 consists of NW-SE trending normal faults and exhibits full-graben geometry (Figs. 6a and 11b; Table 3). Internally graben G6 consists of numerous synthetic and antithetic normal faults. In the center of the graben, a major fault that dips towards the north creates wedge-shaped geometry against the hanging-wall. The seismic facies units show the wedge-shaped configuration in the center of the graben, consisting of inclined, semi-continuous and medium to low amplitude seismic reflections (SF1) (Fig. 11b; Table 2). However, towards the south, the seismic facies units are dominated by semi-continuous, parallel to sub-parallel and medium to low amplitude seismic reflections. Mississippian strata (~1750 ms twt; ~4900 m) were deposited in graben G6. Furthermore, a fold of early Carboniferous age in the center of the graben structure is present against the NW-SE striking normal fault within the Mississippian strata, but the fold structure did not affect the overlying stratigraphic units (Fig. 11b). Towards the northeast, graben G6 is separated from graben G7 by a marginal high, whereas on the high the fault-blocks tilt towards the south.

4.2.7. Graben G7

Graben G7 follows the same trend as graben G4 to the east and the two grabens are separated by a regional high (Figs. 6a and 11d; Table 3). Towards the north, graben G7 is separated from the northeastern Nordkapp sub-basin by a marginal high. The graben is bounded by NW-SE trending master normal faults that dip towards the axis of the structure and create full-graben geometry (Fig. 11d). The observed seismic facies units are composed of semi-continuous to non-continuous, sub-parallel and medium to low amplitude seismic reflections (SF1, Table 2), while the graben structure disappears under the thick pile of salt farther east. Graben G7 accommodated Mississippian strata (~790 ms twt; ~2200 m) of the Billefjorden Group that were deposited under humid, warm and terrestrial environmental conditions during active faulting (Fig. 3).

4.3. Evaporite bodies

During the Pennsylvanian to early Permian (Bashkirian-Asselian), the climate shifted to warm and arid/semi-arid conditions, and facilitated the deposition of warm-water carbonates and sabkha

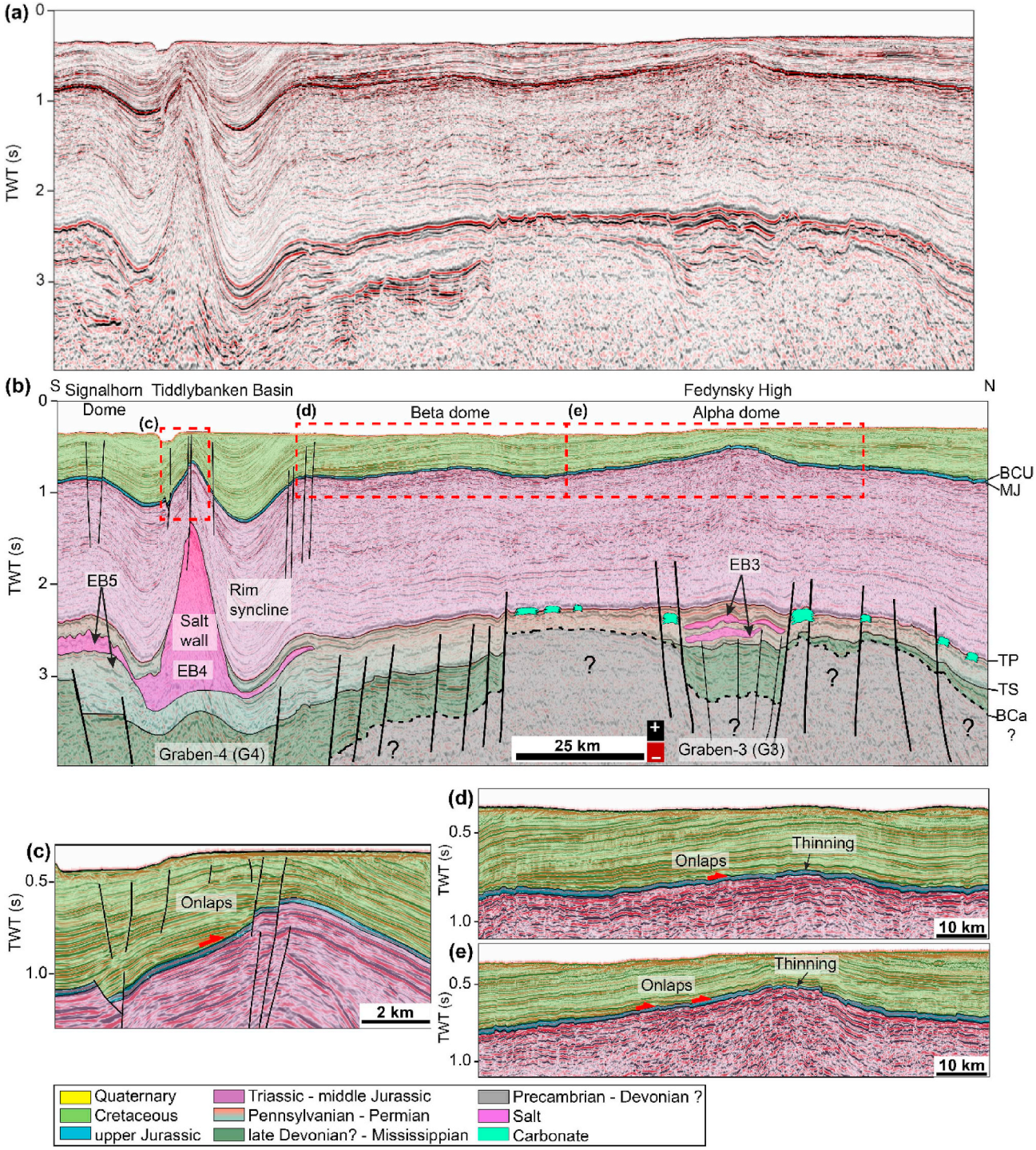

Fig. 8. (a–b) Un-interpreted and interpreted seismic profile, respectively, illustrating the Fedynsky High, Tiddlybanken Basin and Signalhorn Dome with emphasis on the Carboniferous grabens G3-G4, the moderately faulted platform, and the evaporite bodies EB3-EB5; **(c–e)** extracts of the seismic profile illustrating thinning of upper Jurassic strata, and earliest Cretaceous onlaps (small red arrows), respectively; rasters correspond to interpreted sequences (Fig. 3). Profile location in Fig. 1. (For interpretation of the references to colour in this figure legend, the reader is referred to the Web version of this article.)

evaporites of the Gipsdalen Group (e.g. Larssen et al., 2002; Larssen et al., 2005) (Fig. 3). Warm-water and shallow marine carbonates formed at the structural highs and created a barrier for thick halite deposition in the basins (e.g. Rowan and Lindsø, 2017). We were able to identify and constrain five evaporite bodies (EB1 to EB5) within the study area exhibiting contrasting thicknesses and spatial distribution (Table 3). These are affiliated with different structural elements, and they exhibit different seismic facies (Table 2), variable thickness and distribution (Table 4). We observe that the base of the mapped evaporite bodies is relatively flat and less disturbed by faulting in comparison to other pre-salt strata, i.e. in Nordkapp Basin.

4.3.1. *Evaporite body 1 (EB1)*

The evaporite body EB1 is constrained by the master faults of graben G1 and follows the graben boundary limits (Figs. 5, 6b and 7b; Table 4). The horst that separates grabens G1 and G2 has also affected the accumulation of the evaporites. We also observe that over this horst carbonate platforms have formed and separated the evaporite body EB1

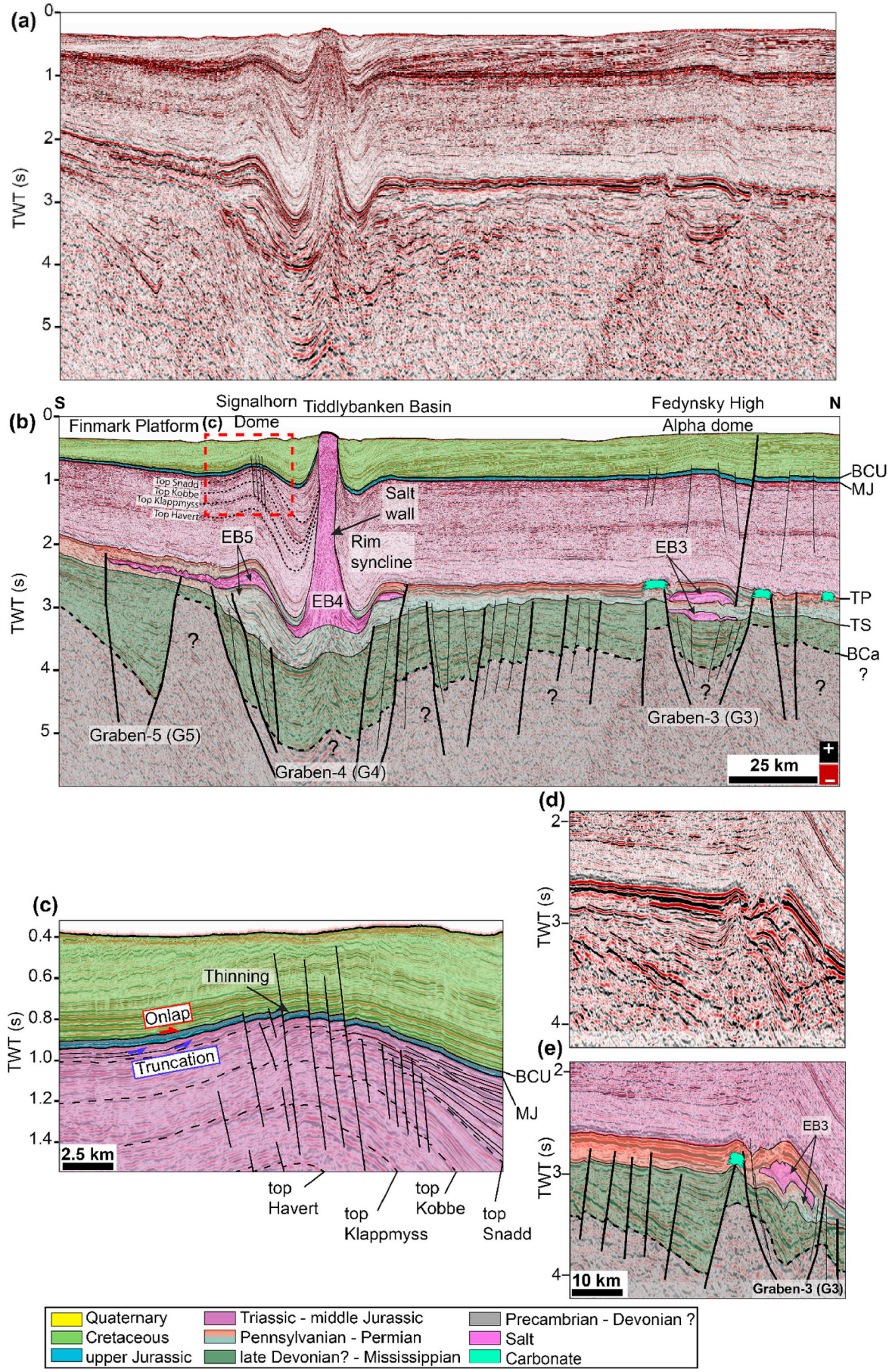

(caption on next page)

Fig. 9. (a–b) Un-interpreted and interpreted seismic profile, illustrating the Fedynsky High, Tiddlybanken Basin, Signalhorn Dome and Finnmark Platform with focus on the Carboniferous grabens G3-G5 and evaporites EB3-EB5; **(c)** extract of the seismic profile demonstrating truncation of uppermost Triassic, thinning of the upper Jurassic strata and lowermost Cretaceous onlap (small red arrow). **(d–e)** Extract of regional profile displays wedge geometry on the west of Fedynsky High, compressed graben G3 and deformed evaporite body EB3; rasters correspond to interpreted sequences (Fig. 3). Profile location in Fig. 1. (For interpretation of the references to colour in this figure legend, the reader is referred to the Web version of this article.)

in graben G1 from the evaporite body EB2 in graben G2 (Fig. 7b). The evaporite body EB1 consists of two facies units, lower and upper, as evidenced by the seismic facies. The lower facies unit is composed of semi-continuous, parallel to sub-parallel and medium to strong amplitude seismic reflections (SF2: ~450 ms time thickness, Fig. 7b; Table 2). For this assemblage, Dellmour et al. (2016) suggested that the prominent reflectivity is related to Gipsdalen Group evaporites dominated by anhydride that is interpreted based on seismic facies (Fig. 7b). The upper facies unit exhibits a featureless, convex upwards and lens-shaped character with the chaotic internal pattern (SF3: ~270 ms time thickness, Table 2). This accordingly have the character of a salt pillow that pinches out at the margins against the master faults of graben G1 (Fig. 7b). The salt pillow is formed on the NW part of the evaporite body EB1 as an irregular, circular-shaped structure while the remaining evaporites dip towards SE (Fig. 6a and b). In map view at the NW part of the evaporite body EB1, a NW-SE trending ridge is evident (Fig. 6b).

4.3.2. Evaporite body 2 (EB2)

The evaporite body EB2 is found inside graben G2 (Figs. 6b and 7b-e; Table 4). On the southeastern part of the graben, the evaporite seismic facies are similar to that of evaporite body EB1 in graben G1 (Fig. 7b). The evaporite body EB2 appears to be flat along the margins of graben G2 (Fig. 7b), while in the central part of the graben, near the northeastern edge of the Nordkapp Basin, the evaporite body is relatively thick and pillow-shaped, suggesting that it represents a transitional lithofacies between mobile halite and non-mobile evaporite (Fig. 7e). The evaporite body EB2 is composed of two facies units that are spatially variable and show a different reflectivity character between the margins and the central part in graben G2. In particular, in the southeastern margin of graben G2, the lower facies unit of the evaporite body EB2 consists of semi-continuous and parallel to sub-parallel seismic reflections (SF2: ~460 ms time thickness, Table 2), while the upper sequence displays a lens-shaped character with chaotic internal pattern (SF3: ~140 ms time thickness, Fig. 7b; Table 2). In the center of the evaporite body, however, the lower facies units comprise non-continuous to diverging seismic reflections (SF2: ~200 ms time thickness, Table 2), whereas the upper facies unit displays a rising pillow-shaped character with medium to high amplitude seismic reflections and chaotic internal patterns (SF3: ~1700 ms time thickness, Fig. 7e; Table 2). The pillow structure shows elongated, asymmetrical geometry and takes a conical-shaped form as it pinches-off at the top (Fig. 6b). The surface morphology of the evaporite body EB2 illustrates that the top of the pillow structure is gentle in the NW-side and steep in the SE-side. Several NE-SW trending depressions are noticeable along the southeastern boundary of the pillow structure (Fig. 6b). We attribute the lower part of the observed seismic facies of the evaporite body EB2 to a layered sequence and non-mobile lithologies, perhaps anhydride, because the seismic expression is similar to the lower sequence of the evaporite body EB1 (Fig. 7b). The upper part of seismic reflections of the evaporite body EB2 with chaotic patterns may represent mobile halite of the Gipsdalen Group.

4.3.3. Evaporite body 3 (EB3)

The evaporite body EB3 is bounded by the master faults of graben G3 and follows the same graben boundary extent (Figs. 6b, 8b and 9b; Table 4). The seismic sections exhibit two lens-shaped pillow structures with chaotic internal patterns (SF3: ~74 ms and ~112 ms time thickness; Table 2). The salt pillows are separated by semi-continuous to sub-parallel seismic reflections with low to medium amplitude (SF2: ~50 ms time thickness, Figs. 8b and 9b; Table 2). The salt pillows are pinching out against the master faults of graben G3. The surface morphology of the evaporite body EB3 suggests that the salt pillows are elongated and dip from southeast towards northwest (Fig. 6b). The upper salt pillow is deformed at the boundary between graben G3 and the northeastern Nordkapp sub-basin (Fig. 9e). On the contrary, the lower salt pillow is prolonged towards the northwest in the middle of graben G3 and becomes perpendicular to the edges of the depression.

4.3.4. Evaporite body 4 (EB4)

Evaporite body EB4 is the thickest of the mapped evaporite structures and was deposited within graben G4 (Figs. 5, 6b and 8b and 9b; Table 4). Together with the evaporite body EB5, they were deposited as one stratigraphic sequence probably belonging to the Gipsdalen Group. The sequence thickens within the central part of graben G4, then thins at the graben margins, and extends farther to the northwest (Fig. 6b). The evaporite bodies EB4 and EB5 were initially part of the same sequence that was eventually split due to the initiation of rim synclines during the early Triassic along the salt wall of the Tiddlybanken Basin. The evaporite body EB4 appears as a salt wall structure in the middle of the Tiddlybanken Basin that has reached the seafloor (Fig. 9b). The salt structure is an isolated, elongated wall that trends NW-SE and shows variable geometry both vertically and spatially (Fig. 5-inset, Figs. 8b and 9b). The salt wall is connected to the source layer and in the central part the stem of the salt wall is narrow in the middle (ca. 2 km width) and forms bulb-shaped geometry at the top (Fig. 5). On the contrary, in the northwestern part of the salt wall the stem is slightly thicker and wider (ca. 5.5 km width) (Fig. 9b). The contact between the salt wall and the Triassic to middle Jurassic strata is spatially variable. The salt wall is internally composed of distorted and chaotic seismic reflections with medium to high amplitude strength (SF3: ~3100 ms time thickness, Table 2). The exact lower limit of this sequence is unknown due to reduced seismic resolution at depth.

4.3.5. Evaporite body 5 (EB5)

The evaporite body EB5 is bounded to the north by the NW-SE trending basin boundary fault of graben G4, while in the south the evaporite body oversteps the southwestern margin of graben G4 (Figs. 6b, 9b and 10b; Table 4). The evaporite body EB5 extends farther above the margins of several graben structures, including grabens G5, G6 and G7, and is connected with the evaporite sequence accumulated in the Nordkapp Basin (Figs. 6b and 11). The thickness of evaporite body EB5 is reduced over the structural highs in comparison to the margins of the graben structures. Internally, the evaporite body EB5 is composed of lower facies units of continuous to semi-continuous, parallel to diverging seismic reflections with medium amplitude strength (SF2: ~900 ms time thickness, Fig. 9b; Table 2). The upper facies units are characterized by several thin pillow-like structures with chaotic internal reflection patterns (SF3: ~226 ms time thickness, Figs. 5, 9b and 10b and 11; Table 2). An elongated, elliptical and NW-SE trending salt anticline covers the western and southwestern margins of graben G4 (Fig. 6b). The mapped surface morphology suggests that the shallowest apex of the salt anticline is parallel to the northwestern segment of the salt wall (Tiddlybanken Basin), while small depressions are formed farther southwest of the NW-SE trending salt anticline (Fig. 6b).

5. Discussion

Seismic interpretation led to detailed mapping of the graben

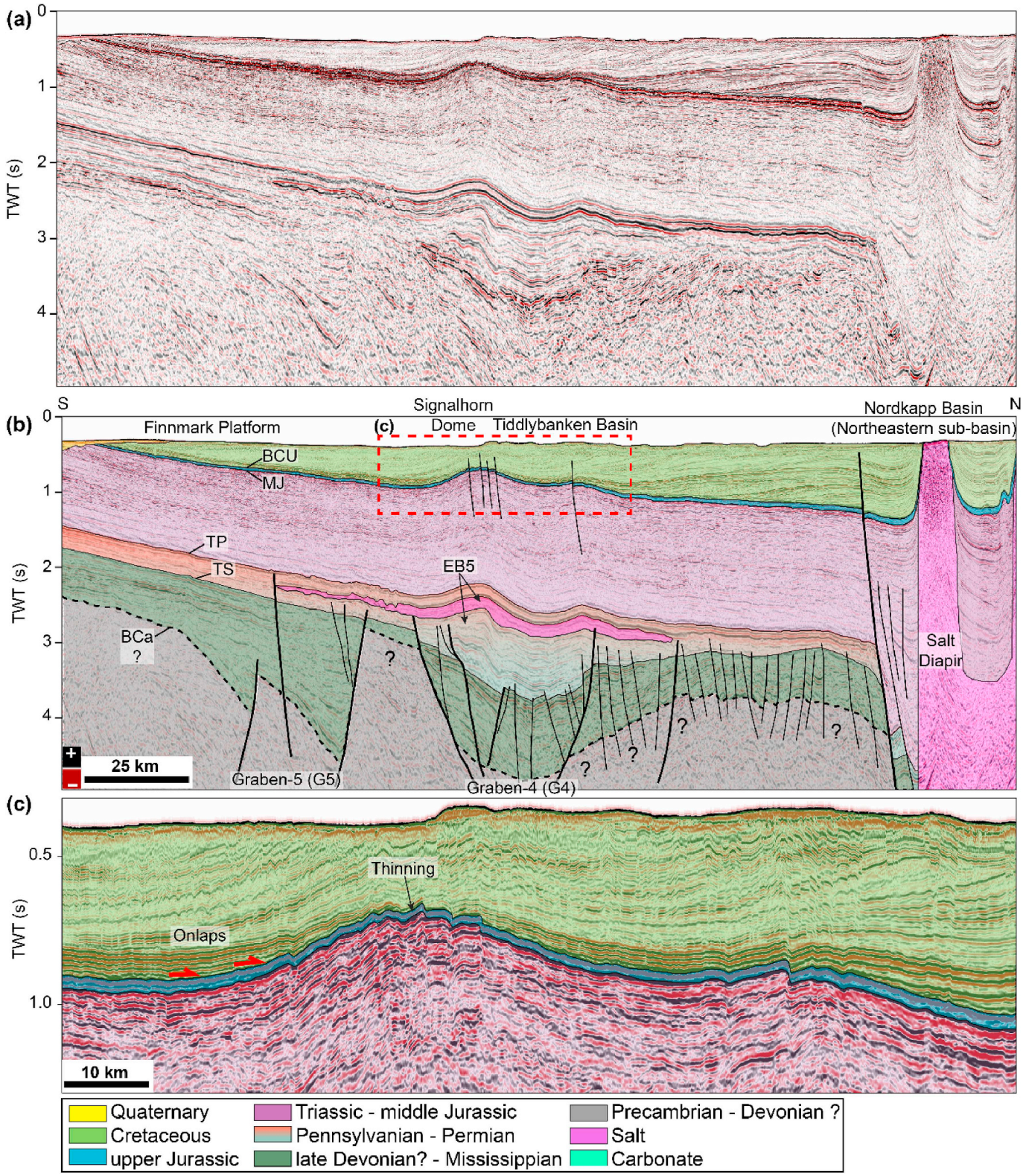

Fig. 10. (a–b) Un-interpreted and interpreted seismic profile, respectively, illustrating the northeastern Nordkapp Basin, Tiddlybanken Basin, Signalhorn Dome and Finnmark Platform with focus on the Carboniferous grabens G4-G5 and evaporite body EB5. Note the folding within the Mississippian strata that affected the entire overburden strata. **(c)** Extract of the seismic profile illustrating thinning of the uppermost Triassic to lowermost Cretaceous successions; small red arrows indicate onlap, while rasters correspond to interpreted sequences (Fig. 3). Profile location in Fig. 1. (For interpretation of the references to colour in this figure legend, the reader is referred to the Web version of this article.)

structures that were dated as late Devonian?-early Carboniferous, and to the correlation of those with the positions of the evaporite bodies and the domes. The evaporite-cored structures in the southeastern Norwegian Barents, including the Haapet, Veslekari, Signalhorn, Alpha and Beta (two domes informally named; composite West Fedynsky) domes, together with the salt wall of the Tiddlybanken Basin, exhibit a

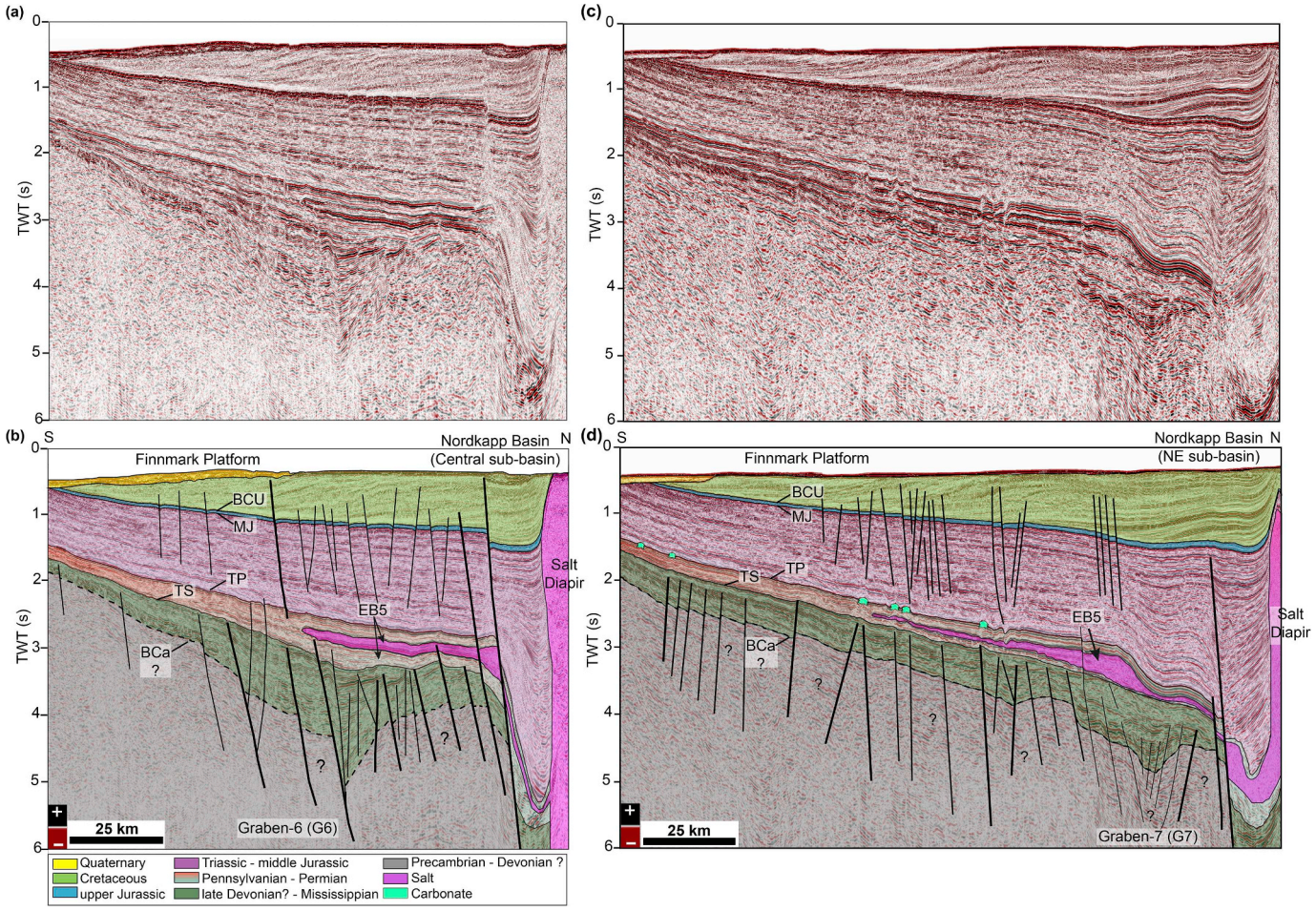

Fig. 11. Un-interpreted and interpreted seismic profile illustrating Carboniferous graben G6-G7 and evaporite body EB5. Graben G6-G7 is buried farther west beneath the thick salt diapirs of the southwestern and central Nordkapp Basin; rasters correspond to interpreted sequences (Fig. 3). Profile location in Fig. 1.

variation of geometries, sizes and orientation (Fig. 12; Table 5). The triggering mechanisms, influence of tectonic inversion, and relations to the deeper structural fabric are generally less well constrained. The structural grain and stress regime that influenced the Carboniferous graben system is discussed in this chapter. We also argue for the possible lithological contrast (mobile and non-mobile) of the accumulated evaporite bodies and their effect on halokinesis, and the causes for triggering and reactivation of evaporite structures in the area.

5.1. Carboniferous evolution

The post-Caledonian and the late Paleozoic basin evolution of the southeastern Norwegian Barents Sea are less well studied in comparison to the western Barents Sea. It is well established that the Carboniferous horst-and-graben basin architecture in the southwestern Barents Sea influenced the sedimentary facies and depositional geometry of the upper Carboniferous to lower Permian evaporites and carbonates (Gudlaugsson et al., 1998; Larssen et al., 2005; Rafaelsen et al., 2008). Based on well-tie and shallow borehole information on the east Finnmark Platform (Bugge et al., 1995), we have identified seven separate grabens beneath the upper Carboniferous to lower Permian evaporite-dominated sequence. The mapped base Carboniferous? (BCa?) reflection provides the deepest mapped level suited to study the basin configuration and to determine the location of the depocenters for the evaporite accumulations. From this, we conclude that the base Carboniferous? (BCa?), top Gipsdalen and Base Cretaceous Unconformity (BCU) time-structure maps can be used to characterize the Carboniferous basins when the evolution of the evaporite-cored domes in the study area are concerned (Figs. 6, 12 and 13).

The Trollfjord-Komagelv Fault Zone (TKFZ) in Finnmark onshore Norway is a NW-SE trending, dextral strike-slip fault and in the southeast, it extends to the Ribachy Peninsula in Russia (Siedlecka, 1975). The TKFZ was particularly active during the late Precambrian to Silurian/Early Devonian and acted as a transform fracture during the opening of the Iapetus Ocean (Johnson et al., 1978; Kjøde et al., 1978; Lippard and Roberts, 1987; Rice et al., 1989; Roberts, 1972; Roberts and Gee, 1985). The zone is the continuation of the Timanian trend onshore northern Norway and it was proposed that its deep roots farther extended to offshore western Barents Sea, i.e. eastern part of Hammerfest Basin and Loppa High (Gabrielsen, 1984; Gabrielsen and Færseth, 1989; Gabrielsen et al., 1990; Karpuz et al., 1993; Lippard and Roberts, 1987). We propose that the same NW-SE trending Timanian structural fabric parallel to the TKFZ (Herrevold et al., 2009) also underlies the southeastern Norwegian Barents Sea and control the structural development of the study region because the trend of all major faults of the graben structures is parallel to the Timanian structural fabric.

The earliest detectable stage of basin formation (late Devonian) in the southeastern Norwegian Barents Sea was characterized by the development of a central structural high (Fedynsky High) and two regional depressions, namely the northern and the southern depressions (Figs. 14a and 15). It is noted that a similar development is recorded during the late Devonian (Famennian) to Mississippian (Visean) widespread across Spitsbergen and the northern Barents Sea that

Table 4
Structural and morphological characteristics of the interpreted evaporite bodies.

Evaporite	Location/Association	Behavior	Associated structure	Lateral extent (km)		Thickness (ms)	
				Length	Width	Margins	Center
Evaporite body 1 (EB1)	Graben 1 and Haapet Dome	Non-mobile	Pillow	~72	~45	~340	~640
Evaporite body 2 (EB2)	Graben 2 and Veslekari Dome	Transitional	Pillow	~103	~49	~600	~2160
Evaporite body 3 (EB3)	Graben 3 and Fedynsky High	Non-mobile	Pillow	~50	~23	~260	~310
Evaporite body 4 (EB4)	Graben 4 and Tiddlybanken Basin	Mobile	Wall	~39	~8	~2000	~3000?
Evaporite body 5 (EB5)	Graben 4 to Graben 7 and Signalhorn Dome, Finnmark Platform and at the margins of the southwestern and central Nordkapp Basin	Non-mobile	Anticline and pillows	~196	~85	**Highs** ~190	**Margins** ~390

accommodated strata of the Billefjorden Group (Cutbill and Challinor, 1965; Gjelberg and Steel, 1981; Smyrak-Sikora et al., 2019). The nature and formation mechanisms of the northern and southern depressions are still unknown, but could be related to a pre-rift stage of crustal thinning during the late Devonian (e.g. Gabrielsen et al., 1985; Nøttvedt et al., 1995) and directly linked to the structural grain of the deep-seated NW-SE trending Timanides. Furthermore, the mylonitic thrust of the so-called Middle Allochthonous Front (MAF) (Fig. 13) represents a major tectonic boundary onshore Finnmark, and separates the Timanian and Caledonian orogenic trends in the offshore domain (Gernigon et al., 2018; Rice and Frank, 2003; Roberts, 1972; Roberts et al., 2011; Roberts and Olovyanishnikov, 2004; Roberts and Siedlecka, 2002; Shulgin et al., 2018) (Fig. 13 inset). The magnetic expression of the Caledonian front (MAF) was interpreted on the Varanger Peninsula based on magnetic data, and appears to have an arch-shaped geometry offshore Finnmark, passing beneath the Central Nordkapp sub-basin (Barrère et al., 2009, 2011; Gernigon and Brönner, 2012; Gernigon et al., 2014, 2018) (Fig. 13).

During the middle-late Devonian, the Pechora Basin was affected by a NE-SW oriented stress regime along with pre-existing Timanian structures (Stoupakova et al., 2011). This extensional phase was also recorded in the eastern Barents Sea during the late Devonian-early Carboniferous and supplemented by magmatism (Ivanova et al., 2011; Nasuti et al., 2015; Petrov et al., 2008; Stoupakova et al., 2011). In the northern part of the East European Craton, Devonian mafic magmatism is exposed in the Timan-Kanin region, the Sredni-Rybachi Peninsula, the Varanger Peninsula and the Digermul Peninsula (Guise and Roberts, 2002; Pease et al., 2016; Roberts and Walker, 1997). Mafic Devonian basalt dykes in the Timan-Kanin region are more similar to the ca. 370 Ma dolerites of the Varanger Peninsula, northern Norway (Pease et al., 2016 and references therein). The source of both episodes of magmatism on the Timan-Kanin and Varanger Peninsula is still debatable. If they are related, it implies regional–scale (ca. 1000 km from Timan-Kanin to the Varanger Peninsula) NNE-SSW rifting of the northern East European Craton (EEC) margin (Pease et al., 2016). Klitzke et al. (2019) also proposed that NE-SW extension related to the deep Paleozoic basins of the Timan-Pechora region reached to the Central Barents Sea, where it reactivated deeper Timanian structures to form the Olga and Sørkapp basins. We suggest that this regional NE-SW oriented stress regime also affected the southeastern Norwegian Barents Sea during the early Carboniferous/Mississippian (Tournaisian-Serpukhovian) and created the NW-SE trending grabens G1-G7. The uniform parallel orientation of the NW-SE striking graben margins (G1-G5) is coherent to an influence of the parallel deep-rooted Timanian structural grain. However, the basement structural grain, may remain dominant in reactivation even in cases where the renewed principle stress deviates significantly from that under which the structures originated (Brun and Tron, 1993; Nur, 1982). Grabens G6 and G7 were also affected by the same stress regime as suggested by the NW-SE trend of the major graben bounding fault (Fig. 6a). However, these structures later became overprinted by the NE-SW trending Nordkapp Basin (Figs. 6a and 13). All grabens (G1-G7) created accommodation space for the deposition of the continental siliciclastic deposits of the Billefjorden Group under humid, warm and terrestrial environmental conditions during the Mississippian active faulting (Stemmerik and Worsley, 2005; Worsley, 2008).

The narrow graben G3 was formed in the Fedynsky High and is the shallowest graben structure (time depth ~3600 ms) in the southeastern Norwegian Barents Sea at base Carboniferous? (BCa?) (Figs. 6, 14b and 15; Table 3). Strata infilling of graben G3 (~600 ms or ~1600 m) is relatively thinner when compared to the other structures, suggesting a strong rheology of the pre-existing structural grain at the Fedynsky High location (Fig. 5). The northern and southern depressions were possibly formed over the weaker zones where the crust was relatively thin due to the late Devonian-early Carboniferous NE-SW oriented extension. The northern depression was further split into grabens G1 and

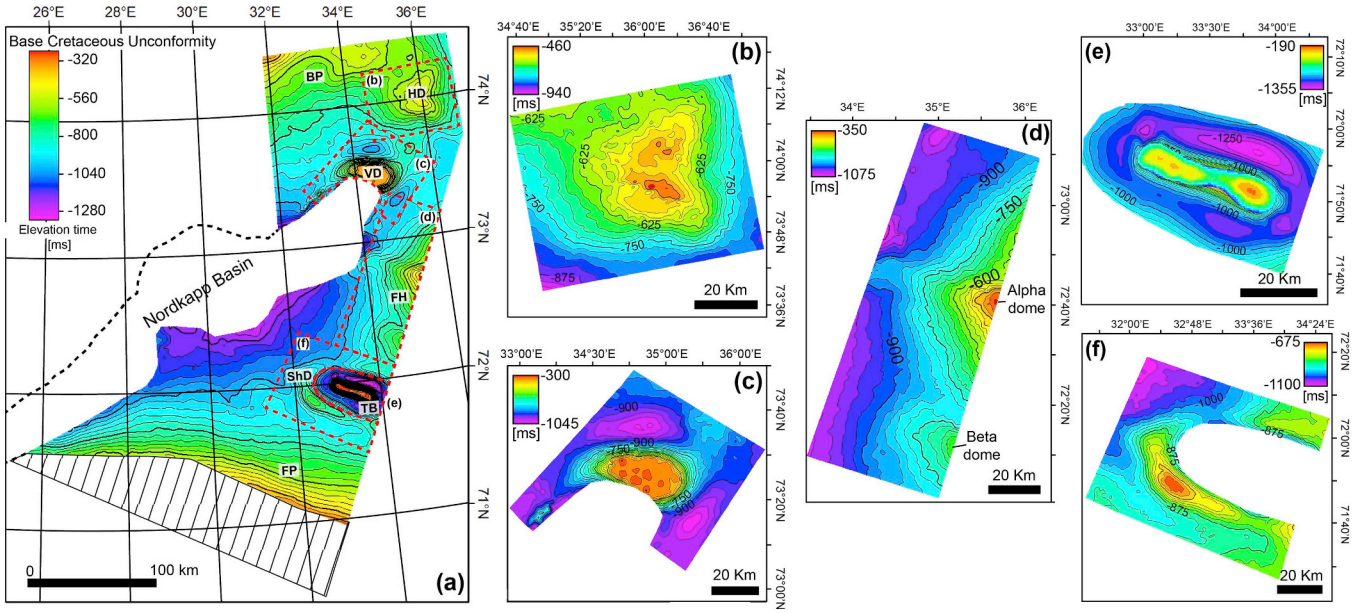

Fig. 12. (a) Base Cretaceous Unconformity (BCU) time-structure map depicting major structural elements in the study area. The dashed region at the southeastern Finnmark Platform demonstrates eroded strata. Red-dotted boxes represent details on: **(b)** Haapet Dome (HD), **(c)** Veslekari Dome (VD), **(d)** Fedynsky High (FH), **(e)** Tiddlybanken Basin (TB), and **(f)** Signalhorn Dome (ShD). Details of the structures described in Table 4. (For interpretation of the references to colour in this figure legend, the reader is referred to the Web version of this article.)

G2. In the southeastern margin, graben G2 is connected to the south with graben G3 (Figs. 6a, 14b and 15). The NW-SE trending graben G2 is separated by a high against the kink of the northeastern Nordkapp Basin, while in the north a NW-SE trending horst is dividing graben G2 from graben G1 (Figs. 6a, 14b and 15). The southern depression is subdivided into a moderately faulted platform and into grabens G4 and G5 that, in turn, became separated by a NW-SE trending horst (Figs. 6a, 14b and 15). Grabens G6 and G7 trend NW-SE and are located at the eastern margins of the southwestern and central Nordkapp sub-basins. However, these grabens were buried farther west beneath the salt structures of the Nordkapp Basin (Figs. 6a and 11). The implication of this is that the basement fabric and Carboniferous grabens G6 and G7 may have affected the segmentation of the Nordkapp Basin (Figs. 6a, 11 and 13).

We observe that the Carboniferous grabens G1-G5 were formed east of the Middle Allochthonous Front (MAF) and above the Timanides (Fig. 13). However, grabens G6 and G7 developed above the frontal Caledonian thrusts, but are still following NW-SE trends, that signifies the control of the older orogen (Figs. 6a and 13). The graben structures have variable intrinsic geometries (e.g. half- and full-graben) and are separated by platforms and structural highs (Figs. 6a and 13). Basin infill is generally thickening towards the axis of the full grabens, except for graben G5 where strata dip to the north and for graben G1 where sedimentary successions dip to the south evidenced by growth strata (Figs. 5 and 7 and 9–11). The dominant NW-SE trend of the Carboniferous grabens has also influenced the deposition of the evaporites in the study region (Figs. 5–11 and 13). However, there is no obvious relation of the rotation of the Middle Allochthonous Front (MAF) or the Timanide/Caledonide transition to the accumulation of the evaporites in the southeastern Norwegian Barents Sea (Fig. 13). All Carboniferous grabens G1-G7 trend orthogonally relative to the axis of the NE-SW striking Nordkapp Basin (Fig. 13). Grabens G6 and G7 of late Devonian?-Mississippian age were directly cross-cut by the NE-SW trending early Pennsylvanian? Nordkapp Basin perhaps due to a change in the stress regime to a NW-SE orientation. Regionally, this temporal change in the stress regime affected the volume accumulation of the evaporites in different depocenters.

5.2. Mobile and non-mobile evaporites

During the Pennsylvanian to early Permian (Bashkirian-Asselian), warm-water carbonates and sabkha evaporites of the Gipsdalen Group were deposited under warm, arid to semi-arid climate and elevated sea-level conditions at approximately 30°N in the sub-tropical zone (Larssen et al., 2005; Stemmerik, 2000) (Fig. 3). Grabens G1-G5 accommodated evaporites, and the thickness and lithological variations of those were dependent on the topography, depositional environment and distance from source areas of the graben structures; e.g. difference in thickness, morphology and facies of the accumulated evaporites between grabens G3 and G4 (Fig. 5) and particular depositional position within each graben (transitional evaporitic facies units in graben G2) (Fig. 7b–e). The thickness, composition and structural position of the accumulated evaporite sequences strongly influenced the basin infilling history and depositional dynamics of the suprasalt strata. Carbonate platforms formed along the edges and the structural highs (SF4, Fig. 5; Table 2). The location of the mapped evaporite bodies EB1-EB4, constrained by the master faults of the equivalent grabens G1-G4, signifies that some of the relief was maintained by the master faults of the graben structures. One exception is the evaporite body EB5 on the southern Finnmark Platform that overstepped the graben margins (G4-G7) and was connected to the southwestern and central parts of the Nordkapp Basin (Fig. 7a and b). The top of evaporite body EB5 is connected with the top of the marginal pillows in the Nordkapp Basin and this shows that evaporite body EB5 was of similar age with the evaporites in the Nordkapp Basin while the thickness and other characteristics are strongly dependent on the basin and structural configuration (Figs. 5, 6b and 13 and 14c; Table 4). However, no clear evidence for faulting has been identified at the base of the evaporite bodies in grabens G1-G5, implying that the evaporite deposition was initiated during the post-rift basin conditions in the southeastern Norwegian Barents Sea (Figs. 5 and 7–10). We argue that the volume of the accumulated evaporites in the Nordkapp Basin and the southeastern Norwegian Barents was strongly influenced by the syn-rift and post-rift basin conditions, respectively.

Salt is mechanically weak layer in comparison to the surrounding lithologies and can flow over the time span of the basin evolution at

Table 5
Structural and morphological characteristics of the Haapet, Veslekari, West Fedynsky (Alpha and Beta, informally named, domes) and Signalhorn domes, and salt wall of the Tiddlybanken Basin.

Structure	Association	Shape in map view (BCU)	Associated structure	Extent (NW-SE) BCU level (km)	Gipsdalen Group level (ms) apex depth	BCU (ms) Apex depth
Haapet Dome	Graben 1 and Evaporite body 1	Irregular, circular	Pillow	~40	~2350	~480
Veslekari Dome	Graben 2 and Evaporite body 2	elliptical	Pillow	~42	~1230	~340
Alpha dome	Graben 3 and Evaporite body 3	elongated	Pillow	~35	~2190	~350
Beta dome	Platform	elliptical	N/A	~13	N/A	~700
Tiddlybanken Basin salt wall	Graben 4 and Evaporite body 4	elongated	Wall	~38	~300	~300
Signalhorn Dome	Graben 4 and Evaporite body 5	elongated, elliptical	Anticline	~58	~2360	~675

particular (> 500 m) burial depths (e.g. Hudec and Jackson, 2007; Jackson and Vendeville, 1994; Jackson and Hudec, 2017; Jackson et al., 1994; Nalpas and Brun, 1993; Vendeville and Jackson, 1992; Withjack and Callaway, 2000). Thick halite-rich and other mobile lithologies are associated with deep basins while thin halite-poor sequences are accommodated at the basin margins and intra-basin structural highs (Clark et al., 1998; Jackson et al., 2018; Kane et al., 2010; Richardson et al., 2005; Rowan, 2014; Rowan and Lindsø, 2017; Stewart et al., 1997). The Gipsdalen Group is well exposed in Central Spitsbergen on Svalbard (Dallmann, 1999; Steel and Worsley, 1984) and on Bjørnøya at the Stappen High (Worsley et al., 2001). These shallow marine sedimentary deposits are further extended to the southwestern Barents Sea and correlated with well and seismic data (Bugge et al., 1995; Ehrenberg et al., 1998; Faleide et al., 1984; Larssen et al., 2005). Seismic data tied to wells and correlations to Spitsbergen suggest that the stratified Gipsdalen Group (Fig. 3) consists of a layered evaporite sequence, composed of a complex interbedded assemblage of evaporites (halite and anhydride) and non-evaporites (carbonate and siliciclastics) in the study area (Table 2). In the southeastern Norwegian Barents Sea, the basins are therefore interpreted to contain a thick sequence of mobile halite, while on the structural highs anhydride (non-mobile) is the dominant lithology (Larssen et al., 2002, 2005; Rafaelsen et al., 2008; Rojo et al., 2019; Rowan and Lindsø, 2017; Samuelsberg et al., 2003).

The five evaporite bodies EB1-EB5 are also composed of rocks correlative to the Gipsdalen Group strata. These display variable internal seismic facies character and thicknesses in the study area. No exploration well has yet penetrated these evaporites in the study area, so that firm lithostratigraphic identification still remains uncertain. We still suggest that evaporite bodies EB1, EB3, and EB5 consist of thin, halite-poor and non-mobile lithologies based on their thickness and seismic signatures (Table 2). Although the evaporite body EB1 was deposited in a graben structure, its salt core is thin with a convex upwards and lens-shaped morphology (Fig. 7b). We observe that this salt-prone lithology constitutes a flat-lying unit on the southeastern extent of the evaporite body EB1 in contrast to the northwestern limits. The thick Gipsdalen Group succession of evaporite body EB1 beneath the salt core is composed of high amplitude, sub-parallel seismic reflections (SF2) (Table 2) and we suggest that this lower part is related to halite-poor and mainly anhydride lithologies (Fig. 7b). Dellmour et al. (2016) also proposed that the lower facies units with prominent reflectivity are related to Gipsdalen Group evaporites dominated by anhydride lithology. The impact of the evaporites EB1 on the evolution of the Haapet Dome is limited as inferred from the E-W oriented section, showing that the anticline is far broader than the evaporite body EB1 (Fig. 16).

The wide anticline of the Haapet Dome can be considered the result of either (1) differential sea-bottom erosion, (2) differential loading, or (3) initial buckling associated with contraction due to the tectonic inversion that is the most likely mechanism for this structure. The growth of the two younger (shallower) anticlines at the margin of the Bjarmeland Platform and the one above the Haapet Dome are younger than the establishment of the Base Cretaceous Unconformity. Neither of those are driven by halokinesis due to non-presence or less thickness of the mobile halite layer, but the Haapet Dome may have been initiated and the growth of it may have been supported by, the existence of the deep, mechanically weak evaporite body. We suggest that the main driving force is the regional tectonic inversion driven by shortening (Fig. 16). We suggest that the evaporite bodies EB1, EB3, and EB5 played a minor role in the evolution of the domes due to their thin sequence thickness and non-mobile lithologies (Fig. 7b–e, 8b, 9b and 10b). Evaporite body EB4 located close and connected with the source layer beneath the Tiddlybanken Basin is halite-rich, as it can be inferred from the salt wall structure and is therefore considered to be mobile (Figs. 5, 8b and 9b). However, the evaporite body EB2 displays an internal transitional seismic signature, which may be related to lithology

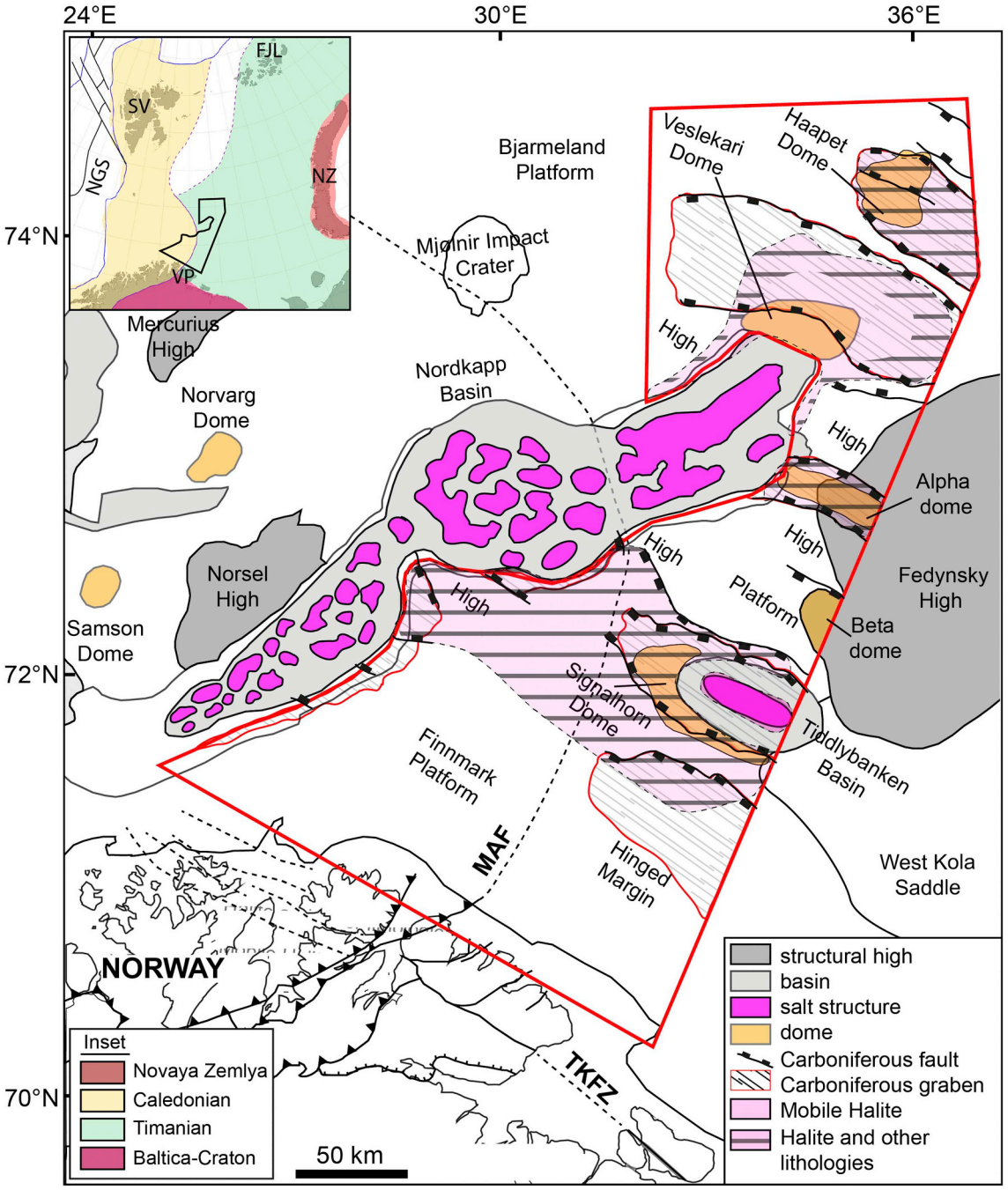

Fig. 13. Overlay of deep-seated Carboniferous grabens G1-G7, evaporite bodies EB1-EB5, and structural elements on the regional geology. Inset: location of the study area at the transition between the Timanian and Caledonian structural fabrics.

variations. At the margins of evaporite body EB2 the halite-rich layer is thin and looks like the remnant of the upper facies unit that thickens towards the center of the graben structure (Fig. 7b–e). The lower layered sequence of evaporite body EB2 exhibits an identical seismic character expression as the evaporite body EB1 and a similar depositional environment for these lower evaporitic units is considered to be likely (Fig. 7b). The flanks of the Veslekari Dome are flat (evaporite body EB2) probably indicating immobile lithologies, perhaps anhydride (Figs. 6b and 7b).

The carbonates of the Gipsdalen Group were deposited at the associated structural highs. However, due to low seismic resolution and lack of 3D seismic data, no platform geometries are observed. During the early to middle Permian (Sakmarian-Kungurian), the depositional environment shifted from warm/arid to temperate conditions due to the northward drift of the southern Barents Sea at approximately 45°N. This allowed for the deposition of cool-water carbonate platforms of the Bjarmeland Group at the primary basin margins (Beauchamp, 1994; Stemmerik, 2000) (Fig. 5). Furthermore, near the top Permian (TP) horizon the Bjarmeland Group carbonates (Fig. 3) show mound geometry with chaotic internal reflection patterns (SF4) (Figs. 5 and 7-9; Table 2). The calculated average thicknesses of the these Bjarmeland Group carbonate platforms at the edges of the different structural features range between ~375 and 610 m (Table 6). It is expected that these mound geometries could consist of multiple stacked carbonate platforms but due to the intrinsic reduced resolution of the available 2D seismic reflection data it is not possible to fully evaluate these features in all details. However, several other studies in the Barents Sea have described and discussed these features in detail together with the

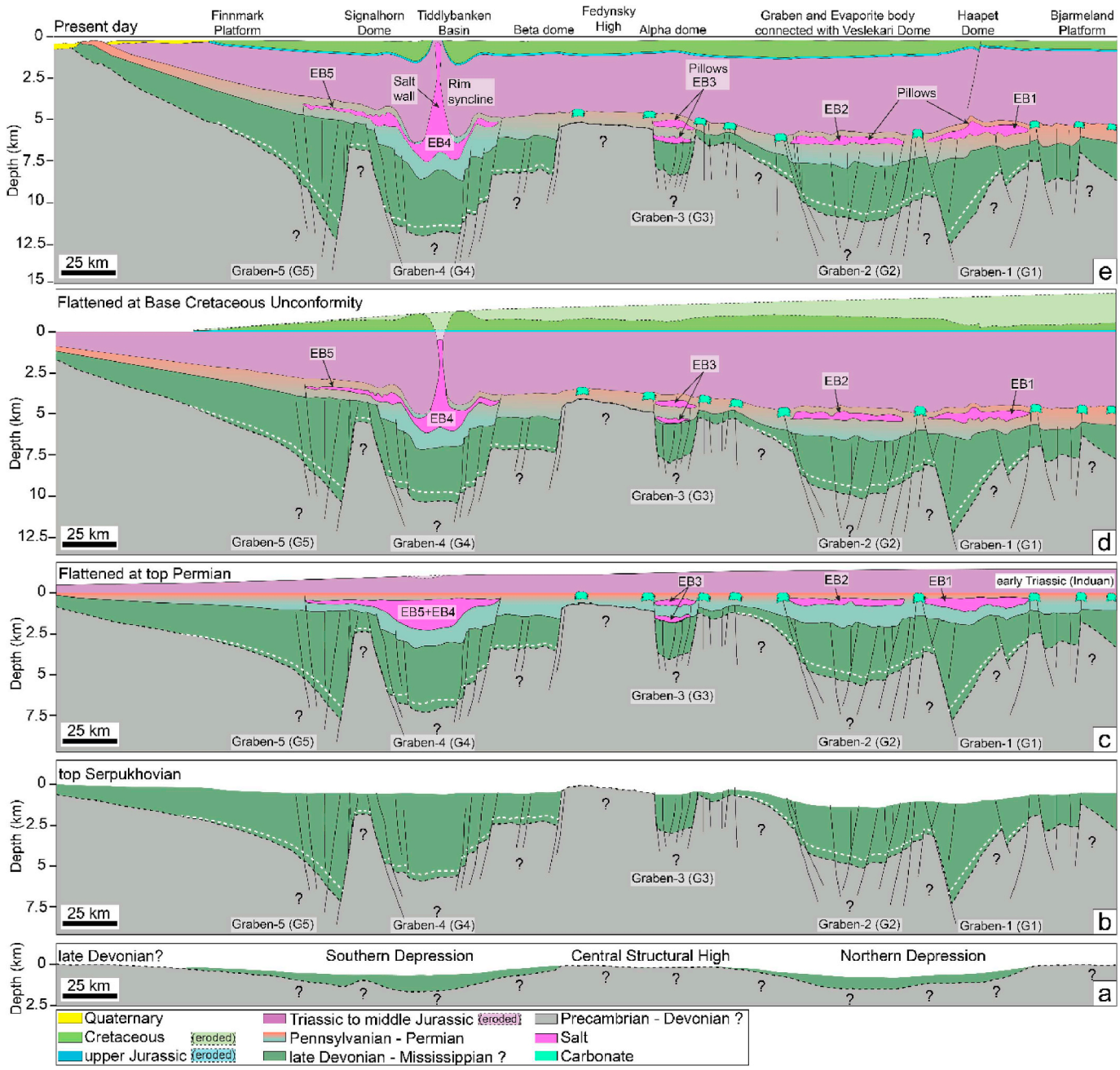

Fig. 14. Late Devonian? to present tectonostratigraphic evolution of the southeastern Norwegian Barents Sea: **(a)** late Devonian?, **(b)** top Serpukhavian, **(c)** flattened at top Permian, **(d)** flattened at Base Cretaceous Unconformity, and **(e)** Present day. Model is based on the depth-converted seismic profile in Fig. 5 utilising the velocity model of Shulgin et al. (2018). Black and white dotted lines illustrate top basement and late Devonian? markers, respectively. Eroded areas are indicated with light colours; rasters correspond to interpreted sequences (Fig. 3). (For interpretation of the references to colour in this figure legend, the reader is referred to the Web version of this article.)

accompanying depositional processes by utilising high resolution 3D seismic data (Alves, 2016, 2019; Colpaert et al., 2007; Mattos et al., 2016; Rafaelsen et al., 2008; Sayago et al., 2018). During the middle to late Permian (Roadian-Changhsigian), the Tempelfjorden Group succession was deposited under regional subsidence conditions over the carbonates (Worsley, 2008) (Fig. 3).

5.3. Tectonic inversion

Triassic sediments, which are sourced from the southeast by the Uralides, were deposited under regional subsidence conditions in the Barents Sea (Glørstad-Clark et al., 2010; Klausen et al., 2015). The development of rim synclines of the Tiddlybanken Basin suggests a transitional syn-kinematic and complex relationship along-strike between the salt wall and the associated early Triassic to middle Jurassic strata for the salt movement (Figs. 5, 8b and 9b). The growth and development of the salt wall probably ceased early at the central and southeastern parts as inferred from the strata thickness variation along the salt wall in the rim synclines (Fig. 5 inset and Fig. 8b) and the outcropping of the upper Triassic to middle Jurassic strata (Fig. 5 inset, Figs. 14d and 15). Later in time, a similar cessation of salt growth is inferred for the northwestern part of the Tiddlybanken Basin (Fig. 9b). As evidenced by the stratal truncations on the southwestern margin of the Tiddlybanken Basin, the Signalhorn Dome was initiated due to the

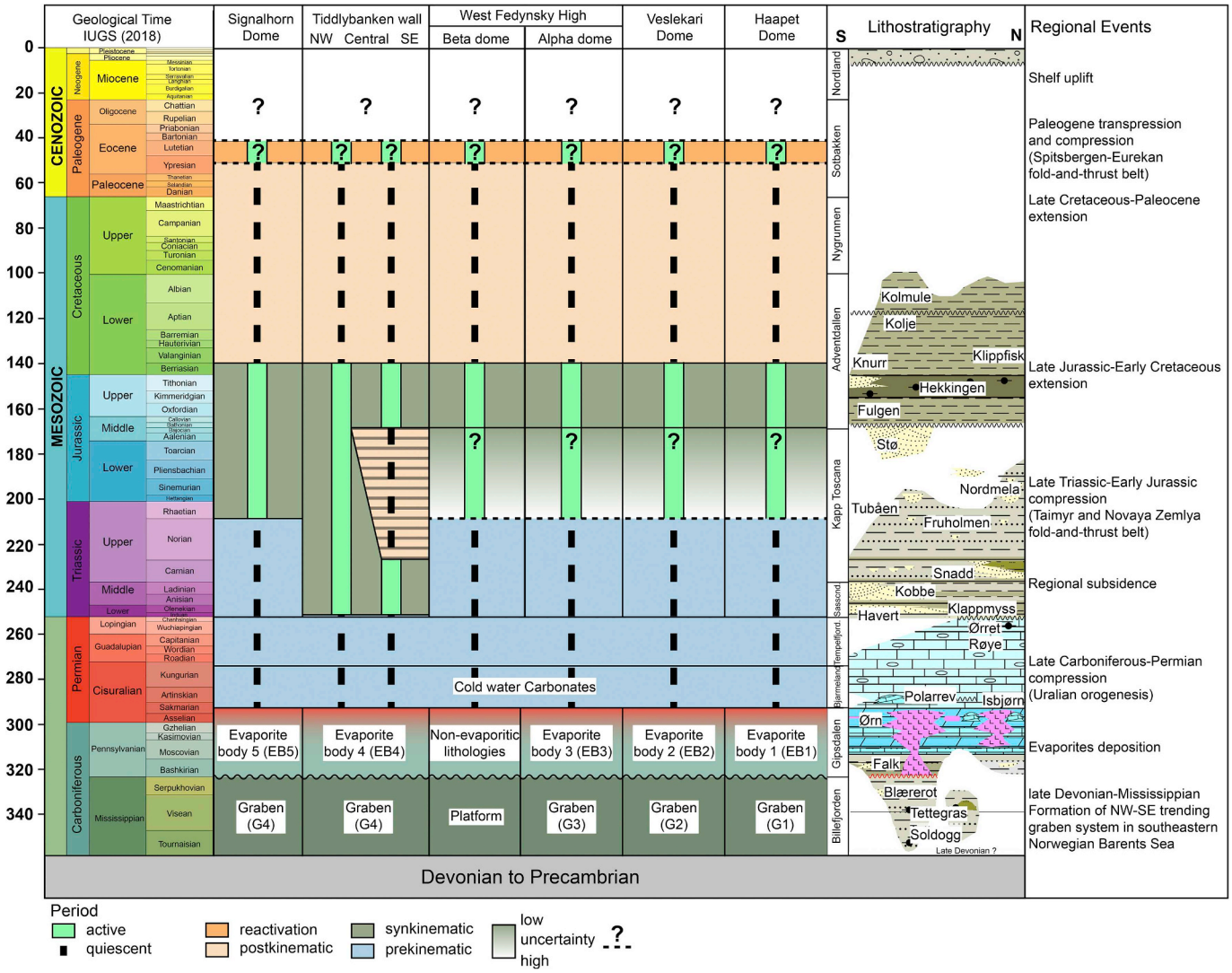

Fig. 15. Growth timing of the evaporite-cored structures in the southeastern Norwegian Barents Sea. Different stages (i.e. prekinematic, synkinematic, postkinematic and reactive) show age relations between the time of overburden deposition and the time of salt flow (Jackson and Talbot, 1991; Jackson and Hudec, 2017). Dashed lines in the postkinematic phase of the central and southeastern part of the Tiddlybanken wall signifies the effect of far-field stress translated from the Novaya Zemlya fold-and-thrust belt.

reactivation of the southwestern master fault of the graben G4 caused by far-field stresses from the Novaya Zemlya fold-and-thrust belt (Fig. 9c). Similarly, the northwestern part of the salt wall was also rejuvenated due to the effect of these far-field stresses as evident by the character of the rim synclines. However, in the central and southeastern parts, this far-field effect could be related to reduced sedimentation rates in the broad palaeo-basin. It implies that the salt movement occurred within the wall from southeast towards the northwest. We argue that the change in the along-strike salt wall development has also affected the evolution of the Signalhorn Dome.

The final up-thrusting of Novaya Zemlya occurred in the Late Triassic (–?Early Jurassic) is well-constrained in reflection seismic (Sobornov, 2013; Sobornov et al., 2015; Stoupakova et al., 2011) and thermochronology data (Zhang et al., 2018). The Rhaetian unconformity known from Svalbard has been connected to the contraction and mountain building in Novaya Zemlya (Müller et al., 2019; Olaussen et al., 2019). In this context, the 200 m-thick estuarine to shoreface deposits of Rhaetian to Pliensbachian age in Kong Karls Land, in comparison to 5 to 20 m-thick condensed succession with eroded strata and numerous hiatuses in western Spitsbergen, are suggested to be the effect of an evolving foreland basin linked to the northern Barents Sea Basin and the Novaya Zemlya fold-and-thrust belt. Similar variations of the deposited successions have been seen in the seismic data of the northern Barents Sea (Olaussen et al., 2019). On Hopen, the Rhaetian unconformity is observed as a subaerial erosive surface where fluvial deposits truncate underlying lower shoreface deposits (Lord et al., in press). Furthermore, results from combined far-field and local (phase-change) stress modeling suggest that the contraction caused by stress related to the development of Novaya Zemlya affected the uplift of the Loppa High (Indrevær et al., 2018). Recent studies over the Svalis Dome in the southwestern Barents Sea using high-resolution shallow reflection data (P-Cable) show an angular unconformity between upper Triassic and lower Jurassic strata on the eastern flank of the structure (Müller et al., 2019). Similarly, higher rates of uplift and erosion over the Fedynsky High were inferred and attributed to the far-field response from the evolving Novaya Zemlya (Müller et al., 2019). The Haapet, Veslekari, Alpha and Beta domes are located in the relative proximity to the Novaya Zemlya fold-and-thrust belt, and this supports the effects of this compressional pulse onto these structures. The compressional stresses in the lower crust transmitted westwards as the stresses were generated from the apex of the stress at Novaya Zemlya fold-and-thrust belt (Indrevær et al., 2017). However, the current resolution of the

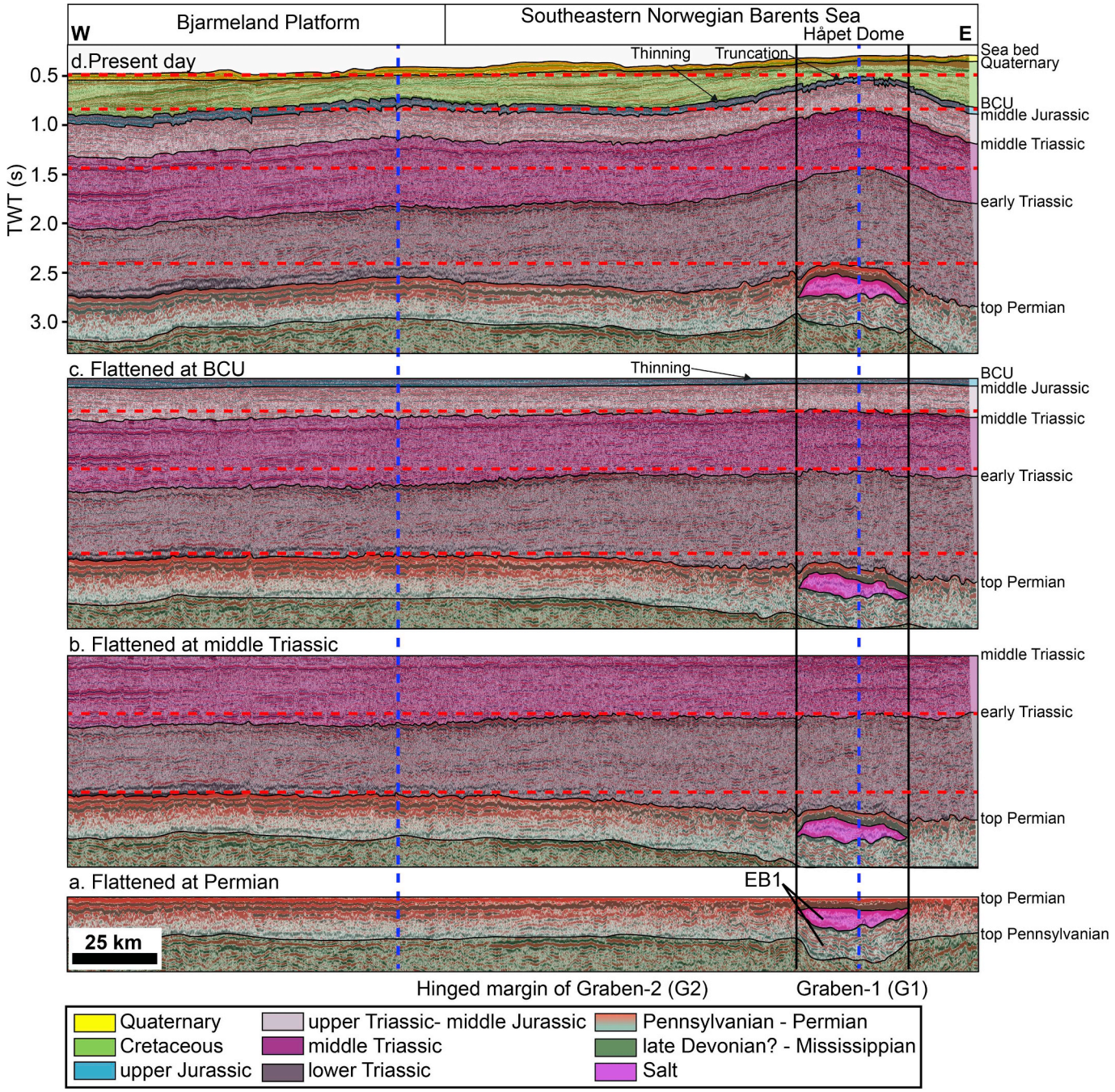

Fig. 16. E-W oriented, interpreted and flattened at different chronological reflections seismic profiles over the Haapet Dome and Bjarmeland illustrating the tectonic control in the study region. The shallower post-BCU anticline above the Haapet Dome is broader than the evaporite body EB1; rasters correspond to interpreted sequences (Fig. 3). Profile location in Fig. 1. Blue and red stipple lines represent the crest of anticline and horizontal to the maximum elevation for a particular surface respectively. (For interpretation of the references to colour in this figure legend, the reader is referred to the Web version of this article.)

utilized 2D seismic dataset is not optimal to decipher in detail this early activity in the southeastern Norwegian Barents. We therefore argue against Mattingsdal et al. (2015) and Rowan and Lindsø (2017) who suggested that the Haapet and Veslekari Domes were instigated during the earliest Cretaceous and post middle Cretaceous, respectively.

The upper Jurassic strata are thinning towards the apex of all structural elements e.g. Haapet, Veslekari, Signalhorn, Alpha and Beta domes, and salt wall (Figs. 7f, 8d-e, 9c, 10c, and 16c-d). However, in some places the lower reflection of the condensed upper Jurassic strata disappears implying that the graben structure was reactivated by the master faults (i.e. graben G4) and created an arch-like feature, i.e. Tiddlybanken Basin and Signalhorn Dome (Fig. 10c). This may be related to the Novaya Zemlya far-field stresses effect, after the erosion of uppermost Triassic strata below the middle Jurassic reflection, as still some topography was maintained by this compressional activity that affected the deposition of upper Jurassic strata (Fig. 10c). During the earliest Cretaceous, all of these positive structures (domes and salt wall) were slightly reactivated as inferred by truncation of upper Jurassic (Figs. 7c and 16d) and onlap to the upper Jurassic strata (Fig. 8c–e, 9c and 10c), except for in the Veslekari Dome, where a 400 km^2 region has been removed by erosion of the earliest Cretaceous (Figs. 7f and 12c). The causes of these mild reactivations are unknown.

A prograding lower Cretaceous shelf-platform complex evolved during the tectonically quiescent period of evaporite-cored structures in

Table 6
Thickness estimations of the Bjarmeland Group carbonates at the edges of the Haapet, Veslekari, Alpha (Fedynsky High) and Signalhorn Domes, and Tiddlybanken Basin. Time thickness (ms) is depth-converted by utilising the velocity model of Shulgin et al. (2018).

Bjarmeland Group carbonate location	TWT (ms)	Thickness (m)
Haapet Dome	200	500
	244	610
Veslekari Dome	242	605
	200	500
Alpha dome (Fedynsky High)	150	375
	229	572.5
Signalhorn Dome	100	250
Tiddlybanken Basin	170	425
	220	550

the southeastern Norwegian Barents Sea (Midtkandal et al., 2019) (Figs. 5, 14d and 15). However, it is unclear whether the upper Cretaceous strata were ever deposited due to the absence of these sequences in the entire southeastern Norwegian Barents Sea. Several studies suggest that 1500–2000 m of Paleogene sediments were deposited and later eroded towards the southeastern Norwegian Barents Sea (Baig et al., 2016; Henriksen et al., 2011b). We propose that the main phase of the reactivation of the domes and the salt wall in close correspondence with the location of the Carboniferous structures occurred in the Paleogene (Figs. 13, 14e and 15). The post-BCU shallow anticline over the Haapet Dome signifies the impact of tectonic inversion as the structure is broader than the evaporite body EB1 (Fig. 16). The Beta dome over the platform in the vicinity of the Fedynsky High is another example of tectonic reactivation as no evaporite body was accumulated in the platform (Fig. 8b and d).

The doming tentatively dated to Paleogene by us, may be related to the Eurekan/Spitsbergen orogeny that took place due to compression caused by the northward movement of Greenland during the early to middle Eocene. The orogen can be traced from North Greenland to Spitsbergen and has extensively shaped the region (Petersen et al., 2016; Piepjohn et al., 2016). It is further associated with dextral strike-slip faulting in Spitsbergen, ultimately linked with the opening of the Norwegian-Greenland Sea and Eurasia Basin (Faleide et al., 2008). We therefore suggest the compressional stresses that reactivated the domes and salt wall within the study area may be related to the transpressional Eurekan/Spitsbergen orogeny. In this context, the post-lower Cretaceous strata were eroded over the Haapet, Signalhorn, Alpha and Beta domes due to the imposed tectonic inversion and reactivation during the early-middle Eocene as a far-field response to the Eurekan/Spitsbergen orogenic event (Figs. 7c, 8d-e, 10c, 14e, 15 and 16d). Upper Triassic to Cretaceous strata also subcrop at the seafloor above the Veslekari Dome (Fig. 7f). In contrast, uppermost Triassic to Cretaceous strata (Fig. 5 inset) and upper Jurassic to Cretaceous successions (Fig. 9b), in the central/southeast and in the northwest, respectively, are tilted and subcrop to the seafloor along the rejuvenated complex salt wall of the Tiddlybanken Basin due to the suggested early-middle Eocene inversion (Figs. 15 and 16). However, the exact timing of the imposed compressional deformation within the early-middle Eocene is challenging to be constrained in detail only considering the study area as the entire Paleogene succession is missing.

6. Conclusions

1. During the late Devonian, the study area was dominated by a central structural high region (Fedynsky High) rimmed by depressions to its north and south. We suggest that the late Devonian-early Carboniferous (Mississippian) NE-SW oriented stress regime, as suggested for the evolution of the Pechora Basin, eastern Barents Sea, and Olga-Sørkapp region also, created the NW-SE striking graben structures (G1-G7) in the southeastern Norwegian Barents Sea, mainly exploiting the Timanian Orogen structural grain.
2. Pennsylvanian to early Permian evaporite units (EB1-EB5) were deposited thereafter. The discrepancy in syn-rift to post-rift basin conditions affected the distribution and thickness of the accumulated evaporites, partly or fully occupying the available accommodation space. The deep-seated structures constrained the accumulation and facies variations of the evaporites and strongly controlled the distribution and partially the evolution of the stratigraphically shallower domes. The effect of salt mobilization on the dome evolution depended on the relative amount of lithologies with mobile to immobile properties, and the relative stratigraphic thickness of each unit.
3. The NW-SE trending salt wall evolution within the Tiddlybanken Basin is complex, varies along-strike, and has affected the structural development of the Signalhorn Dome. The Haapet, Veslekari, Alpha, Beta and Signalhorn domes were instigated and the salt wall was rejuvenated during the late Triassic due to compressional stresses propagating from the Novaya Zemlya fold-and-thrust belt.
4. All of the structural elements were mildly reactivated during the upper Jurassic and earliest Cretaceous. During the early Cretaceous prograding shelf-platform complex buried the domes and the salt wall until reactivation of the deep-seated Carboniferous grabens led to the reactivation of these structures and to the erosion of the post-lower Cretaceous strata over their crest.
5. We infer an early-middle Eocene timing for the main phase of reactivation of the domes and salt wall, probably in response to regional compressional stresses related to the transpressional Eurekan/Spitsbergen orogeny.

Conflicts of interest

The authors declare that they have no conflict of interest.

Declarations of interest

None.

Acknowledgments

The present study is part of the ARCEx project (Research Centre for Arctic Petroleum Exploration), which is funded by the Research Council of Norway (grant number 228107) together with ten academic and six industry partners (Equinor, Vår Energi, AkerBP, Lundin Norway, OMV and Wintershall DEA). We want to thank all the academic institutes, industry and funding partners. Vår Energi is acknowledged for sponsoring the Adjunct Professor position of F. Tsikalas at the University of Oslo. Schlumberger are thanked for providing academic license to the Petrel© software. The Norwegian Petroleum Directorate (NPD), TGS-NOPEC Geophysical Company ASA, and Spectrum Geo are also acknowledged for access to the regional seismic data. Reviews by Cathy Hollis and an anonymous reviewer, with editorial remarks from Tiago M. Alves helped to improve the manuscript. However, the technical contents and ideas presented herein are solely the authors' interpretations.

Appendix A. Supplementary data

Supplementary data to this article can be found online at https://doi.org/10.1016/j.marpetgeo.2019.104038.

References

Alves, T.M., 2016. Polygonal mounds in the Barents Sea reveal sustained organic productivity towards the P–T boundary. Terra. Nova 28, 50–59.
Alves, T., 2019. Paleozoic carbonates record the 4D evolution of salt domes in the Barents Sea. In: 81st EAGE Conference and Exhibition 2019.

Anell, I.M., Faleide, J.I., Braathen, A., 2016. Regional tectono-sedimentary development of the highs and basins of the northwestern Barents Shelf. Nor. Geol. Tidsskr. 96, 27–41.
Baig, I., Faleide, J.I., Jahren, J., Mondol, N.H., 2016. Cenozoic exhumation on the southwestern Barents Shelf: estimates and uncertainties constrained from compaction and thermal maturity analyses. Mar. Pet. Geol. 73, 105–130.
Barrère, C., Ebbing, J., Gernigon, L., 2009. Offshore prolongation of Caledonian structures and basement characterisation in the western Barents Sea from geophysical modelling. Tectonophysics 470, 71–88.
Barrère, C., Ebbing, J., Gernigon, L., 2011. 3-D density and magnetic crustal characterization of the southwestern Barents Shelf: implications for the offshore prolongation of the Norwegian Caledonides. Geophys. J. Int. 184, 1147–1166.
Beauchamp, B., 1994. Permian Climatic Cooling in the Canadian Arctic, vol. 288. Geological Society of America Special Paper, pp. 229–246.
Blaich, O., Tsikalas, F., Faleide, J., 2017. New insights into the tectono-stratigraphic evolution of the southern stappen high and its transition to Bjørnøya basin, SW Barents Sea. Mar. Pet. Geol. 85, 89–105.
Breivik, A.J., Gudlaugsson, S.T., Faleide, J.I., 1995. Ottar Basin, SW Barents Sea: a major Upper Palaeozoic rift basin containing large volumes of deeply buried salt. Basin Res. 7, 299–312.
Breivik, A.J., Mjelde, R., Grogan, P., Shimamura, H., Murai, Y., Nishimura, Y., 2005. Caledonide development offshore–onshore Svalbard based on ocean bottom seismometer, conventional seismic, and potential field data. Tectonophysics 401, 79–117.
Breivik, A.J., Mjelde, R., Grogan, P., Shimamura, H., Murai, Y., Nishimura, Y., Kuwano, A., 2002. A possible Caledonide arm through the Barents Sea imaged by OBS data. Tectonophysics 355, 67–97.
Brun, J.-P., Tron, V., 1993. Development of the north viking graben: inferences from laboratory modelling. Sediment. Geol. 86, 31–51.
Bugge, T., Mangerud, G., Elvebakk, G., Mørk, A., Nilsson, I., Fanavoll, S., Vigran, J.O., 1995. The upper Palaeozoic succession on the Finnmark platform, Barents Sea. Nor. Geol. Tidsskr. 75, 3–30.
Clark, J., Stewart, S., Cartwright, J., 1998. Evolution of the NW margin of the north Permian basin, UK north sea. J. Geol. Soc. 155, 663–676.
Colpaert, A., Pickard, N., Mienert, J., Henriksen, L.B., Rafaelsen, B., Andreassen, K., 2007. 3D seismic analysis of an upper Palaeozoic carbonate succession of the eastern Finnmark platform area, Norwegian Barents Sea. Sediment. Geol. 197, 79–98.
Cutbill, J., Challinor, A., 1965. Revision of the stratigraphical scheme for the Carboniferous and Permian rocks of spitsbergen and Bjørnøya. Geol. Mag. 102, 418–439.
Dallmann, W.K., 1999. Lithostratigraphic Lexicon of Svalbard: Review and Recommendations for Nomenclature use: Upper Palaeozoic to Quaternary Bedrock. Norsk Polarinstitut.
Dellmour, R., Stueland, E., Lindstrom, S., Tari, G., Purkis, S., 2016. The håpet dome in the Norwegian Barents Sea, structural evolution and morphometry of salt basins. In: 78th EAGE Conference and Exhibition 2016-Workshops.
Dimakis, P., Braathen, B.I., Faleide, J.I., Elverhøi, A., Gudlaugsson, S.T., 1998. Cenozoic erosion and the preglacial uplift of the Svalbard–Barents Sea region. Tectonophysics 300, 311–327.
Drachev, S., Malyshev, N., Nikishin, A., 2010. Tectonic History and Petroleum Geology of the Russian Arctic Shelves: an Overview, Geological Society, London, Petroleum Geology Conference Series. Geological Society of London, pp. 591–619.
Ehrenberg, S.N., Nielsen, E., Svånå, T.A., Stemmerik, L., 1998. Depositional evolution of the Finnmark carbonate platform, Barents Sea: results from wells 7128/6-1 and 7128/4-1. Nor. Geol. Tidsskr. 78, 185–224.
Eldholm, O., Tsikalas, F., Faleide, J., 2002. Continental Margin off Norway 62–75 N: Palaeogene Tectono-Magmatic Segmentation and Sedimentation, vol. 197. Geological Society, London, Special Publications, pp. 39–68.
Faleide, J.I., Gudlaugsson, S.T., Jacquart, G., 1984. Evolution of the western Barents Sea. Mar. Pet. Geol. 1, 123–150.
Faleide, J.I., Pease, V., Curtis, M., Klitzke, P., Minakov, A., Scheck-Wenderoth, M., Kostyuchenko, S., Zayonchek, A., 2018. Tectonic implications of the lithospheric structure across the Barents and Kara shelves. Geol. Soc. Lond. Spec. Publ. 460, 285–314.
Faleide, J.I., Tsikalas, F., Breivik, A.J., Mjelde, R., Ritzmann, O., Engen, O., Wilson, J., Eldholm, O., 2008. Structure and evolution of the continental margin off Norway and the Barents Sea. Episodes 31, 82–91.
Faleide, J.I., Vågnes, E., Gudlaugsson, S.T., 1993. Late Mesozoic-Cenozoic evolution of the south-western Barents Sea in a regional rift-shear tectonic setting. Mar. Pet. Geol. 10, 186–214.
Gabrielsen, R., 1984. Long-lived fault zones and their influence on the tectonic development of the southwestern Barents Sea. J. Geol. Soc. 141, 651–662.
Gabrielsen, R., Færseth, R.B., 1989. The inner shelf of North Cape, Norway and its implications for the Barents Shelf-Finnmark Caledonide boundary. A comment. Nor. Geol. Tidsskr. 69, 57–62.
Gabrielsen, R., Kløvjan, O., Rasmussen, A., Stølan, T., 1992. Interaction between halokinesis and faulting: structuring of the margins of the Nordkapp Basin, Barents Sea region. In: Proceedings Structural and tectonic modelling and its implication to petroleum geology; proceedings1992, vol. 1. pp. 121–131.
Gabrielsen, R.H., Faerseth, R.B., Jensen, L.N., 1990. Structural Elements of the Norwegian Continental Shelf. Pt. 1. The Barents Sea Region. Norwegian Petroleum Directorate.
Gabrielsen, R.H., Grunnaleite, I., Rasmussen, E., 1997. Cretaceous and tertiary inversion in the Bjørnøyrenna Fault Complex, south-western Barents Sea. Mar. Pet. Geol. 14, 165–178.
Gabrielsen, R.H., Ulvøen, S., Elvsborg, A., Ekern, O.F., 1985. The Geological History and Geochemical Evaluation of Block 2/2, Offshore Norway, Petroleum Geochemistry in Exploration of the Norwegian Shelf. Springer, pp. 165–178.
Gee, D., Bogolepova, O., Lorenz, H., 2006. The Timanide, Caledonide and Uralide Orogens in the Eurasian High Arctic, and relationships to the Palaeo-Continents Laurentia, Baltica and Siberia. Geol. Soc. Lond. Mem. 32, 507–520.
Gee, D.G., Fossen, H., Henriksen, N., Higgins, A.K., 2008. From the early Paleozoic platforms of Baltica and Laurentia to the caledonide orogen of scandinavia and Greenland. Episodes 31, 44–51.
Gernigon, L., Brönner, M., 2012. Late Palaeozoic architecture and evolution of the southwestern Barents Sea: insights from a new generation of aeromagnetic data. J. Geol. Soc. 169, 449–459.
Gernigon, L., Brönner, M., Dumais, M.-A., Gradmann, S., Grønlie, A., Nasuti, A., Roberts, D., 2018. Basement inheritance and salt structures in the SE Barents Sea: insights from new potential field data. J. Geodyn.
Gernigon, L., Brönner, M., Roberts, D., Olesen, O., Nasuti, A., Yamasaki, T., 2014. Crustal and basin evolution of the southwestern Barents Sea: from Caledonian orogeny to continental breakup. Tectonics 33, 347–373.
Gjelberg, J., Steel, R., 1981. An Outline of Lower-Middle Carboniferous Sedimentation on Svalbard: Effects of Tectonic, Climatic and Sea Level Changes in Rift Basin Sequences.
Glørstad-Clark, E., Faleide, J.I., Lundschien, B.A., Nystuen, J.P., 2010. Triassic seismic sequence stratigraphy and paleogeography of the western Barents Sea area. Mar. Pet. Geol. 27, 1448–1475.
Green, P., Duddy, I., 2010. Synchronous exhumation events around the Arctic including examples from Barents Sea and Alaska north slope. In: Geological Society, London, Petroleum Geology Conference Series. Geological Society of London, pp. 633–644.
Gudlaugsson, S., Faleide, J., Johansen, S., Breivik, A., 1998. Late Palaeozoic structural development of the south-western Barents Sea. Mar. Pet. Geol. 15, 73–102.
Guise, P.G., Roberts, D., 2002. Devonian ages from 40Ar/39Ar dating of plagioclase in dolerite dykes, eastern Varanger Peninsula, North Norway. Nor. Geol. Unders. Bull. 440, 27–37.
Henriksen, E., Bjørnseth, H., Hals, T., Heide, T., Kiryukhina, T., Kløvjan, O., Larssen, G., Ryseth, A., Rønning, K., Sollid, K., 2011b. Uplift and Erosion of the Greater Barents Sea: Impact on Prospectivity and Petroleum Systems. vol. 35. Geological Society, London, pp. 271–281 Memoirs.
Henriksen, E., Ryseth, A., Larssen, G., Heide, T., Rønning, K., Sollid, K., Stoupakova, A., 2011a. Tectonostratigraphy of the Greater Barents Sea: Implications for Petroleum Systems. vol. 35. Geological Society, London, pp. 163–195 Memoirs.
Herrevold, T., Gabrielsen, R.H., Roberts, D., 2009. Structural geology of the southeastern part of the Trollfjorden-Komagelva Fault zone, varanger peninsula, Finnmark, north Norway. Nor. J. Geol./Norsk Geol. Foren. 89.
Hudec, M.R., Jackson, M.P., 2007. Terra infirma: understanding salt tectonics. Earth Sci. Rev. 82, 1–28.
Indrevær, K., Gac, S., Gabrielsen, R.H., Faleide, J.I., 2017. Crustal-scale subsidence and uplift caused by metamorphic phase changes in the lower crust: a model for the evolution of the Loppa High area, SW Barents Sea from late Paleozoic to Present. J. Geol. Soc. jgs2017–2063.
Indrevær, K., Gac, S., Gabrielsen, R.H., Faleide, J.I., 2018. Crustal-scale subsidence and uplift caused by metamorphic phase changes in the lower crust: a model for the evolution of the Loppa High area, SW Barents Sea from late Paleozoic to present. J. Geol. Soc. 175, 497–508.
Ivanova, N., Sakulina, T., Belyaev, I., Matveev, Y.I., Roslov, Y.V., 2011. Depth model of the Barents and Kara Seas according to geophysical surveys results. Geol. Soc., Lond., Mem. 35, 209–221.
Jackson, C.A.L., Elliott, G.M., Royce-Rogers, E., Gawthorpe, R.L., Aas, T.E., 2018. Salt Thickness and Composition Influence Rift Structural Style, Northern North Sea, Offshore Norway. Basin Research.
Jackson, M.P., Talbot, C.J., 1991. A Glossary of Salt Tectonics. Bureau of Economic Geology, University of Texas at Austin, pp. 44 Geologic Circular 91-4.
Jackson, M.P., Vendeville, B., 1994. Regional extension as a geologic trigger for diapirism. Geol. Soc. Am. Bull. 106, 57–73.
Jackson, M.P., Hudec, M.R., 2017. Salt Tectonics: Principles and Practice. Cambridge University Press.
Jackson, M.P., Vendeville, B.C., Schultz-Ela, D.D., 1994. Structural dynamics of salt systems. Annu. Rev. Earth Planet Sci. 22, 93–117.
Johnson, H., Levell, B., Siedlecki, S., 1978. Late Precambrian sedimentary rocks in East Finnmark, north Norway and their relationship to the Trollf jord-Komagelv fault. J. Geol. Soc. 135, 517–533.
Kane, K.E., Jackson, C.A.-L., Larsen, E., 2010. Normal fault growth and fault-related folding in a salt-influenced rift basin: south Viking Graben, offshore Norway. J. Struct. Geol. 32, 490–506.
Karpuz, M., Roberts, D., Olesen, O., Gabrielsen, R., Herrevold, T., 1993. Application of multiple data sets to structural studies on Varanger Peninsula, Northern Norway. Int. J. Remote Sens. 14, 979–1003.
Kjøde, J., Storetvedt, K., Roberts, D., Gidskehaug, A., 1978. Palaeomagnetic evidence for large-scale dextral movement along the Trollfjord-Komagelv Fault, Finnmark, north Norway. Phys. Earth Planet. Inter. 16, 132–144.
Klausen, T.G., Ryseth, A.E., Helland-Hansen, W., Gawthorpe, R., Laursen, I., 2015. Regional development and sequence stratigraphy of the middle to late Triassic snadd formation, Norwegian Barents Sea. Mar. Pet. Geol. 62, 102–122.
Klitzke, P., Franke, D., Ehrhardt, A., Lutz, R., Reinhardt, L., Heyde, I., Faleide, J., 2019. The Paleozoic evolution of the Olga basin region, northern Barents Sea–a link to the Timanian orogeny. Geochem. Geophys. Geosyst.
Knutsen, S.-M., Larsen, K., 1997. The late Mesozoic and Cenozoic evolution of the Sørvestsnaget Basin: a tectonostratigraphic mirror for regional events along the Southwestern Barents Sea margin? Mar. Pet. Geol. 14, 27–54.
Kostyuchenko, S., Sapozhnikov, R., Egorkin, A., Gee, D., Berzin, R., Solodilov, L., 2006. Crustal structure and tectonic model of northeastern Baltica, based on deep seismic and potential field data. Geol. Soc., Lond., Mem. 32, 521–539.

Kristensen, T.B., Rotevatn, A., Marvik, M., Henstra, G.A., Gawthorpe, R.L., Ravnås, R., 2018. Structural evolution of sheared margin basins: the role of strain partitioning. Sørvestsnaget Basin, Norwegian Barents Sea. Basin Res. 30, 279–301.
Larssen, G., Elvebakk, G., Henriksen, L., Kristensen, S., Nilsson, I., Samuelsberg, T., Svånå, T., Stemmerik, L., Worsley, D., 2005. Upper Palaeozoic lithostratigraphy of the southern part of the Norwegian Barents Sea. Bull. - Norges Geol. Undersokelse 444.
Larssen, G., Elvebakk, G., Henriksen, L.B., Kristensen, S., Nilsson, I., Samuelsberg, T., Svånå, T., Stemmerik, L., Worsley, D., 2002. Upper Palaeozoic lithostratigraphy of the southern Norwegian Barents Sea. Nor. Pet. Dir. Bull. 9, 76.
Lasabuda, A., Laberg, J.S., Knutsen, S.-M., Høgseth, G., 2018a. Early to middle Cenozoic paleoenvironment and erosion estimates of the southwestern Barents Sea: insights from a regional mass-balance approach. Mar. Pet. Geol.
Lasabuda, A., Laberg, J.S., Knutsen, S.-M., Safronova, P., 2018b. Cenozoic tectonostratigraphy and pre-glacial erosion: a mass-balance study of the northwestern Barents Sea margin, Norwegian Arctic. J. Geodyn. 119, 149–166.
Leever, K.A., Gabrielsen, R.H., Faleide, J.I., Braathen, A., 2011. A transpressional origin for the West Spitsbergen fold-and-thrust belt: insight from analog modeling. Tectonics 30.
Lippard, S., Roberts, D., 1987. Fault systems in Caledonian Finnmark and the southern Barents Sea. Nor. Geol. Unders. Bull. 410, 55–64.
Lord, G.S., Mørk, M.B.E., Mørk, A., Olaussen, S., 2019. Sedimentology and petrography of the svenskøya formation on hopen, svalbard: an analogue to sandstone reservoirs in the realgrunnen subgroup. Polar Research 38. https://doi.org/10.33265/polar.v38.3523.
Marello, L., Ebbing, J., Gernigon, L., 2010. Magnetic basement study in the Barents Sea from inversion and forward modelling. Tectonophysics 493, 153–171.
Marello, L., Ebbing, J., Gernigon, L., 2013. Basement inhomogeneities and crustal setting in the Barents Sea from a combined 3D gravity and magnetic model. Geophys. J. Int. 193, 557–584.
Mattingsdal, R., Høy, T., Simonstad, E., Brekke, H., 2015. An updated map of structural elements in the southern Barents Sea. In: 31st Geological Winter Meeting, pp. 12–14.
Mattos, N.H., Alves, T.M., Omosanya, K.O., 2016. Crestal fault geometries reveal late halokinesis and collapse of the Samson Dome, Northern Norway: implications for petroleum systems in the Barents Sea. Tectonophysics 690, 76–96.
Midtkandal, I., Faleide, T.S., Faleide, J.I., Planke, S., Anell, I., Nystuen, J.P., 2019. Nested intrashelf platform clinoforms—evidence of shelf platform growth exemplified by Lower Cretaceous strata in the Barents Sea. Basin Res.
Müller, R., Klausen, T., Faleide, J., Olaussen, S., Eide, C., Suslova, A., 2019. Linking regional unconformities in the Barents Sea to compression-induced forebulge uplift at the Triassic-Jurassic transition. Tectonophysics.
Nalpas, T., Brun, J.-P., 1993. Salt flow and diapirism related to extension at crustal scale. Tectonophysics 228, 349–362.
Nasuti, A., Roberts, D., Gernigon, L., 2015. Multiphase mafic dykes in the Caledonides of northern Finnmark revealed by a new high-resolution aeromagnetic dataset. Nor. J. Geol./Norsk Geol. Foren. 95.
Nur, A., 1982. The origin of tensile fracture lineaments. J. Struct. Geol. 4, 31–40.
Nøttvedt, A., Gabrielsen, R., Steel, R., 1995. Tectonostratigraphy and sedimentary architecture of rift basins, with reference to the northern North Sea. Mar. Pet. Geol. 12, 881–901.
Olaussen, S., Larssen, G.B., Helland-Hansen, W., Johannessen, E.P., Nøttvedt, A., Riis, F., Rismyhr, B., Smelror, M., Worsley, D., 2019. Mesozoic strata of Kong Karls Land, svalbard, Norway; a link to the northern Barents Sea basins and platforms. Nor. J. Geol./Norsk Geol. Foren. 98.
Pease, V., Drachev, S., Stephenson, R., Zhang, X., 2014. Arctic lithosphere—a review. Tectonophysics 628, 1–25.
Pease, V., Gee, D., Lopatin, B., 2001. Is Franz Josef Land Affected by Caledonian Deformation? EUG XI Abstract.
Pease, V., Scarrow, J., Silva, I.N., Cambeses, A., 2016. Devonian magmatism in the Timan Range, Arctic Russia—subduction, post-orogenic extension, or rifting? Tectonophysics 691, 185–197.
Petersen, T.G., Thomsen, T., Olaussen, S., Stemmerik, L., 2016. Provenance shifts in an evolving Eurekan foreland basin: the tertiary central basin, spitsbergen. J. Geol. Soc. 173, 634–648.
Petrov, O.V., Sobolev, N.N., Koren, T.N., Vasiliev, V.E., Petrov, E.O., Birger Larssen, G., Smelror, M., 2008. Palaeozoic and early mesozoic evolution of the east Barents and Kara seas sedimentary basins. Nor. J. Geol./Norsk Geol. Foren. 88.
Piepjohn, K., von Gosen, W., Tessensohn, F., 2016. The Eurekan deformation in the Arctic: an outline. J. Geol. Soc. 173, 1007–1024.
Rafaelsen, B., Elvebakk, G., Andreassen, K., Stemmerik, L., Colpaert, A., Samuelsberg, T.J., 2008. From detached to attached carbonate buildup complexes—3D seismic data from the upper Palaeozoic, Finnmark Platform, southwestern Barents Sea. Sediment. Geol. 206, 17–32.
Rice, A., Frank, W., 2003. The early Caledonian (Finnmarkian) event reassessed in Finnmark: 40Ar/39Ar cleavage age data from NW Varangerhalvøya, N. Norway. Tectonophysics 374, 219–236.
Rice, A., Gayer, R., Robinson, D., Bevins, R., 1989. Strike-slip restoration of the Barents Sea Caledonides Terrane, Finnmark, north Norway. Tectonics 8, 247–264.
Richardson, N.J., Underhill, J.R., Lewis, G., 2005. The role of evaporite mobility in modifying subsidence patterns during normal fault growth and linkage, Halten Terrace, Mid-Norway. Basin Res. 17, 203–223.
Riis, F., Lundschien, B.A., Høy, T., Mørk, A., Mørk, M.B.E., 2008. Evolution of the Triassic shelf in the northern Barents Sea region. Polar Res. 27, 318–338.
Ritzmann, O., Faleide, J.I., 2007. Caledonian basement of the western Barents Sea. Tectonics 26.
Ritzmann, O., Faleide, J.I., 2009. The crust and mantle lithosphere in the Barents Sea/Kara Sea region. Tectonophysics 470, 89–104.
Roberts, D., 1972. Tectonic deformation in the Barents Sea Region of Varanger peninsula. Universitetsforlaget, Finnmark.
Roberts, D., Chand, S., Rise, L., 2011. A half-graben of inferred Late Palaeozoic age in outer Varangerfjorden, Finnmark: evidence from seismic reflection profiles and multibeam bathymetry. Nor. J. Geol./Norsk Geol. Foren. 91.
Roberts, D., Gee, D.G., 1985. An introduction to the structure of the Scandinavian caledonides. The Caled. Orog.–Scand. Relat. Areas 1, 55–68.
Roberts, D., Olovyanishnikov, V., 2004. Structural and tectonic development of the Timanide orogen. Geol. Soc., Lond., Mem. 30, 47–57.
Roberts, D., Siedlecka, A., 2002. Timanian orogenic deformation along the northeastern margin of Baltica, northwest Russia and northeast Norway, and Avalonian–Cadomian connections. Tectonophysics 352, 169–184.
Roberts, D., Walker, N., 1997. U-Pb zircon age of a dolerite dyke from near Hamninberg, Varanger Peninsula, North Norway. and its regional significance. Nor. Geol. Unders. 432, 95–102.
Rojo, L.A., Cardozo, N., Escalona, A., Koyi, H., 2019. Structural style and evolution of the Nordkapp Basin, Norwegian Barents Sea. AAPG (Am. Assoc. Pet. Geol.) Bull.
Ronnevik, H., Beskow, B., Jacobsen, H.P., 1982. Structural and Stratigraphic Evolution of the Barents Sea.
Rowan, M., 2014. Passive-margin salt basins: hyperextension, evaporite deposition, and salt tectonics. Basin Res. 26, 154–182.
Rowan, M., Lindsø, S., 2017. Salt Tectonics of the Norwegian Barents Sea and Northeast Greenland Shelf, Permo-Triassic Salt Provinces of Europe, North Africa and the Atlantic Margins. Elsevier, pp. 265–286.
Ryseth, A., Augustson, J.H., Charnock, M., Haugerud, O., Knutsen, S.-M., Midbøe, P.S., Opsal, J.G., Sundsbø, G., 2003. Cenozoic stratigraphy and evolution of the sørvestsnaget basin, southwestern Barents Sea. Nor. J. Geol./Norsk Geol. Foren. 83.
Samuelsberg, T.J., Elvebakk, G., Stemmerik, L., 2003. Late Palaeozoic evolution of the Finnmark platform, southern Norwegian Barents Sea. Nor. J. Geol./Norsk Geol. Foren. 83.
Sayago, J., Di Lucia, M., Mutti, M., Sitta, A., Cotti, A., Frijia, G., 2018. Late Paleozoic seismic sequence stratigraphy and paleogeography of the paleo-Loppa High in the Norwegian Barents Sea. Mar. Pet. Geol. 97, 192–208.
Shulgin, A., Mjelde, R., Faleide, J.I., Høy, T., Flueh, E., Thybo, H., 2018. The crustal structure in the transition zone between the western and eastern Barents Sea. Geophys. J. Int. 214, 315–330.
Siedlecka, A., 1975. Late Precambrian stratigraphy and structure of the north-eastern margin of the Fennoscandian Shield (east Finnmark-timan region). Nor. Geol. Unders. 316, 313–348.
Sigmond, E.M., 2003. Geological Map, Land and Sea Areas of Northern Europe. Norges geologiske undersøkelse.
Smyrak-Sikora, A., Johannessen, E.P., Olaussen, S., Sandal, G., Braathen, A., 2019. Sedimentary architecture during Carboniferous rift initiation–the arid Billefjorden trough, svalbard. J. Geol. Soc. 176, 225–252.
Sobornov, K., 2013. Structure and petroleum habitat of the Pay Khoy-Novaya Zemlya Foreland Fold belt, Timan Pechora, Russia. AAPG Search Discov. Artic. 10554.
Sobornov, K., Afanasenkov, A., Gogonenkov, G., 2015. Strike-slip faulting in the northern part of the west siberian basin and Enisey-Khatanga trough: structural expression, development and implication for petroleum exploration. In: 3P Arctic Conference Search and Discovery Article.
Steel, R.J., Worsley, D., 1984. Svalbard's Post-caledonian Strata—An Atlas of Sedimentational Patterns and Palaeogeographic Evolution, Petroleum Geology of the North European Margin. Springer, pp. 109–135.
Stemmerik, L., 2000. Late Palaeozoic evolution of the north Atlantic margin of Pangea. Palaeogeogr. Palaeoclimatol. Palaeoecol. 161, 95–126.
Stemmerik, L., Worsley, D., 2005. 30 years on-Arctic Upper Palaeozoic stratigraphy, depositional evolution and hydrocarbon prospectivity. Nor. J. Geol./Norsk Geol. Foren. 85.
Stewart, S., Ruffell, A., Harvey, M., 1997. Relationship between basement-linked and gravity-driven fault systems in the UKCS salt basins. Mar. Pet. Geol. 14, 581–604.
Stoupakova, A., Henriksen, E., Burlin, Y.K., Larsen, G., Milne, J., Kiryukhina, T., Golynchik, P., Bordunov, S., Ogarkova, M., Suslova, A., 2011. The geological evolution and hydrocarbon potential of the Barents and Kara shelves. Geol. Soc., Lond., Mem. 35, 325–344.
Tsikalas, F., Faleide, J.I., Eldholm, O., Blaich, O.A., 2012. The NE Atlantic Conjugate Margins, Regional Geology and Tectonics: Phanerozoic Passive Margins, Cratonic Basins and Global Tectonic Maps. Elsevier, pp. 140–201.
Tsikalas, F., Blaich, O.A., Faleide, J.I., Olaussen, S., 2019. Stappen high-Bjørnøya tectonosedimentary element, Barents Sea. In: Drachev, S., Henriksen, E., Brekke, H. (Eds.), Arctic Sedimentary Basins. Geological Society of London, Books (in press).
Vendeville, B.C., Jackson, M.P., 1992. The rise of diapirs during thin-skinned extension. Mar. Pet. Geol. 9, 331–354.
Withjack, M.O., Callaway, S., 2000. Active normal faulting beneath a salt layer: an experimental study of deformation patterns in the cover sequence. AAPG Bull. 84, 627–651.
Worsley, D., 2008. The post-Caledonian development of Svalbard and the western Barents Sea. Polar Res. 27, 298–317.
Worsley, D., Agdestein, T., Gjelberg, J.G., Kirkemo, K., Mørk, A., Nilsson, I., Olaussen, S., Steel, R.J., Stemmerik, L., 2001. The geological evolution of Bjørnøya, Arctic Norway: implications for the Barents shelf. Nor. J. Geol./Norsk Geol. Foren. 81.
Zattin, M., Andreucci, B., de Toffoli, B., Grigo, D., Tsikalas, F., 2016. Thermochronological constraints to late Cenozoic exhumation of the Barents Sea shelf. Mar. Pet. Geol. 73, 97–104.
Zhang, X., Pease, V., Carter, A., Scott, R., 2018. Reconstructing Palaeozoic and Mesozoic tectonic evolution of Novaya Zemlya: combing geochronology and thermochronology. Geol. Soc. Lond. Spec. Publ. 460, 335–353.